Hydrol. Earth Syst. Sci. Discuss., 10, 7235–7290, 2013
www.hydrol-earth-syst-sci-discuss.net/10/7235/2013/
doi:10.5194/hessd-10-7235-2013


Hydrology and Earth System Sciences
Open Access
Discussions



# An interdisciplinary swat ecohydrological model to define catchment-scale hydrologic partitioning

**C. L. Shope[1,*], G. R. Maharjan[2], J. Tenhunen[2], B. Seo[2], K. Kim[2], J. Riley[2], S. Arnhold[3], T. Koellner[4], Y. S. Ok[5], S. Peiffer[1], B. Kim[6], J.-H. Park[7], and B. Huwe[3]**

[1]Univ. of Bayreuth, Dept. of Hydrology, Universitatstrasse 30, 95440 Bayreuth, Germany
[2]Univ. of Bayreuth, Dept. of Plant Ecology, Universitatstrasse 30, 95440 Bayreuth, Germany
[3]Univ. of Bayreuth, Dept. of Soil Physics, Universitatstrasse 30, 95440 Bayreuth, Germany
[4]Univ. of Bayreuth, Professorship of Ecosystem Services, Universitatstrasse 30, 95440 Bayreuth, Germany
[5]Department of Biological Environment, Kangwon National University, 192-1 Hyoja-Dong, Gwangwon-do, Chuncheon 200-701, South Korea
[6]Kangwon Nat. Univ., Dept. of Env. Science, 192-1 Hyoja-Dong, Gwangwon-do, Chuncheon, 200-701, Republic of Korea
[7]EWHA Womans Univ. Dept. of Environmental Science and Engineering, Seoul 120-750, Republic of Korea
[*]now at: US Geological Survey, 2329 Orton Circle, Salt Lake City, UT, USA







Received: 12 March 2013 – Accepted: 8 May 2013 – Published: 6 June 2013

Correspondence to: C. L. Shope (cshope@usgs.gov)

Published by Copernicus Publications on behalf of the European Geosciences Union.







## Abstract

Land use and climate change have long been implicated in modifying ecosystem services, such as water quality and water yield, biodiversity, and agricultural production. To account for future effects on ecosystem services, the integration of physical, biological, economic, and social data over several scales must be implemented to assess the effects on natural resource availability and use. Our objective is to assess the capability of the SWAT model to capture short-duration monsoonal rainfall-runoff processes in complex mountainous terrain under rapid, event-driven processes in a monsoonal environment. To accomplish this, we developed a unique quality-control gap-filling algorithm for interpolation of high frequency meteorological data. We used a novel multi-location, multi-optimization calibration technique to improve estimations of catchment-wide hydrologic partitioning. We calibrated the interdisciplinary model to a combination of statistical, hydrologic, and plant growth metrics. In addition, we used multiple locations of different drainage area, aspect, elevation, and geologic substrata distributed throughout the catchment. Results indicate scale-dependent sensitivity of hydrologic partitioning and substantial influence of engineered features. While our model accurately reproduced observed discharge variability, the addition of hydrologic and plant growth objective functions identified the importance of culverts in catchment-wide flow distribution. The results of this study provide a valuable resource to describe landscape controls and their implication on discharge, sediment transport, and nutrient loading. This study also shows the challenges of applying the SWAT model to complex terrain and extreme environments. By incorporating anthropogenic features into modeling scenarios, we can greatly enhance our understanding of the hydroecological impacts on ecosystem services.





HESSD

10, 7235–7290, 2013



## 1 Introduction

Land use and climate change have been implicated in reduced ecosystem services such as high quality water yield, biodiversity, and agricultural production from the local to the global scale (Reid et al., 2010). Recently, these research studies have focused on the integration of land-use decision making and ecosystem services tradeoffs (Goldstein et al., 2012). The crop/land use distribution can have a substantial influence on the overall catchment water balance due to precipitation interception, evaporation, transpiration, soil moisture redistribution, and temporal variation in surface runoff associated with crop development. The effects of land use change, including deforestation (Forti et al., 1995), agricultural intensification (Berka et al., 2001), yearly variations in agricultural land use (Tilman et al., 2002), and construction of roads, culverts, and sediment detention ponds (Forman and Alexander, 1998), on stream discharge and water quality occur at a variety of spatial and temporal scales. Deforestation significantly affects streamflow characteristics (Calder, 1992) by increasing erosion and decreasing soil moisture and soil nutrient concentrations; while agricultural intensification affects surface runoff by altering infiltration, evaporation, and timing of runoff. The agricultural intensification effects can be compounded by double cropping systems (Calder, 1992). Therefore, the prediction of ecosystem services expected under future land use decisions and changing climate conditions has become increasingly important. These complex policy and management decisions require the integration of not only physical processes, but the inclusion of robust economic and social data over a range of scales to assess the effects on water resource allocation and ecologic behavior. As agricultural land use increases, the need for water resources management increases, particularly in complex topography driven by extreme events, where water management becomes an increasingly important factor in obtaining desired ecosystem services.

A coupled hydrological and crop production model is an efficient approach to simulate the interactions of catchment physical characteristics, agricultural practices, and weather inputs on the water yield, biogeochemistry, sediment transport and agricultural





HESSD
10, 7235–7290, 2013



economic gains. Calibrated watershed-scale models are a useful tool for understanding management practices and the consequences of land use and climate change (Pieri et al., 2007) and to evaluate conservation practices in locations with limited observational data (Cho et al., 2012). Further, model scenarios can be helpful in identifying reasonable measures for assessing environmental ecological status while taking into account relevant factors like climate, land distribution, and water use (Lam et al., 2012; Krysanova et al., 2005). Watershed simulation models are commonly separated into either ecologic or hydrologic investigations (Kumar and Duffy, 2009; Xu et al., 2012a; Hellebrand and van den Bos, 2008). By incorporating both ecological and hydrologic data into a single modeled system, the number of modeled parameters increases as well as the spatial and temporal discretization. However, with increased discretization, more physical observational data are necessary, leading to over-parameterization and scaling issues (Doherty, 2003). It is crucial to find the balance between the number of parameters and model sensitivity to support the model objectives (Xu et al., 2012a).

Due to the complexity of large-scale multi-objective analyses, numerical and distributed watershed models are typically highly parameterized and manual calibration can be virtually impossible (Schuol and Abbaspour, 2006). While manual calibration is useful to understand the importance of specific parameters in the watershed, multi-site, multi-objective inverse calibration and uncertainty analysis can aid in understanding the system (Abbaspour et al., 2004; Duan et al., 2003). Borah and Bera (2004) found that the distributed Soil and Water Assessment Tool (SWAT) model was a promising long-term simulation code for predominately agricultural watersheds when compared to several other integrated watershed models. However, in their study, daily flow calibration and validation was found to be less precise than monthly comparisons (Borah and Bera, 2004; Spruill et al., 2000). SWAT has also been successfully applied in a wide variety of data-limited studies, particularly in South Korea (Lee et al., 2012; Lee et al., 2011; Stehr et al., 2008; Mekonnen et al., 2009).

The water resources of the Haean catchment in South Korea are important to quantify because the catchment represents an important contributor to the Han River and





HESSD
10, 7235–7290, 2013



the Soyang Lake watershed, which is a major drinking water source for major metropolitan areas including the city of Seoul (Jo and Park, 2010). In addition, the catchment is a significant source of sediment and nutrients due to the high agricultural activity and forest encroachment (Jung et al., 2012; Lee et al., 2013). Locally, the social structure and livelihood depends highly on the quantity and quality of the Mandae Stream and its tributaries where, small-scale agriculture is the largest economic activity within the basin, engaging 85 % of the population and 54 % of the available land area within the catchment. Increasing agricultural encroachment into the forest region imposes a significant risk to water yield and quality. Over the past 20 yr, the Haean land use/land cover change in the forested region has steadily reduced forested area by 37 % with an increase in major crops like radish, potato, and western cabbage and more recently in high-value orchard and ginseng crops (Kim et al., 2011). Furthermore, routing and flow management for many of these crops has induced row and furrow cultivation procedures with plastic mulching, which has been shown to significantly increase the erosive power and decreased infiltration of individual events (Arnhold et al., 2013). Previous studies have also suggested an appreciable decline in aquatic species, attributed in large part to an increase in fine grain sediment erosion and nutrient concentrations (Jun, 2009; B. Kim, personal communication, 2011). Since the end of the Korean War in 1953, a variety of amelioration measures such as river regulation, installation of catchment drainage systems, and waste water treatment plants (WWTPs) have been implemented in order to enlarge communities and increase local agricultural production. These measures have led to a change in the catchment-wide water balance, spatiotemporal nutrient dynamics, and floodplain ecology (Jun, 2009) and therefore, research and management in these areas is increasingly important (Tenhunen et al., 2011). Several conservation projects have been implemented within the Haean catchment and throughout South Korea to limit and effectively manage soil erosion including retention pond construction, modification of riparian channel widths, and channel reinforcement engineering. Consequently, the landscape has been intensively altered through agricultural management, surface flow routing, and engineering design,





HESSD
10, 7235–7290, 2013



which has created a mosaic of ecohydrologic landscape patterns. Therefore, accurately modeling the hydrologic characteristics throughout the catchment is the first step in agricultural pollution identification and mitigation.

Throughout the Haean catchment, surface water flow has been observed to be entirely depleted over extended stretches due to domestic and irrigation abstractions (Shope et al., 2013). However, irrigation for agricultural crops may not be dependent on surface water but instead obtained through groundwater abstraction, particularly irrigated rice and orchard farming. The surface water and groundwater abstractions, dam and reservoir operations, and engineered hydraulic structures (culverts, sediment ponds, and roads) have greatly disrupted the natural hydrology of the catchment. Previous research has indicated that seasonal precipitation as well as individual events influence the hydrologic flushing of organic materials from the land surface (Jung et al., 2012; Lee et al., 2013), similar to the dilution of dissolved ions observed in other studies (i.e., Murdoch et al., 2000). In addition, the long-term interdisciplinary research group TERRECO (Tenhunen et al., 2011), has collected spatiotemporal terrestrial surface runoff measurements to calculate sediment yield (Arnhold et al., 2013), invoked dye tracer experiments to estimate soil structure and variably saturated flow and transport processes (Ruidisch et al., 2013), and examined the implications of groundwater and surface water exchange on spatiotemporal fluxes and near-stream biogeochemistry (Bartsch et al., 2013). To quantify overland runoff, sediment transport, and soil loss from individual crops under specific management practices, it is critical to understand sustainable resource allocation and scenario implications in this agriculturally productive, complex terrain.

This study builds upon multiple research investigations distributed throughout the Soyang Lake watershed and we implement the SWAT ecohydrologic model within the Haean catchment to quantify hydrologic processes and catchment-wide flow partitioning. Our objectives are to (1) characterize the spatiotemporal river discharge patterns at multiple locations throughout the monsoon driven catchment through multi-objective optimization, (2) assess the potential of a spatiotemporal algorithm to improve





HESSD
10, 7235–7290, 2013



discretization of thoroughly monitored precipitation, (3) determine the capability of the SWAT model to capture short-duration monsoonal rainfall-runoff processes in the complex mountainous terrain of the Haean catchment from the daily perspective, and (4) quantify the significance of engineered structures (roads, culverts, sedimentation ponds) on flow partitioning throughout the catchment. To accomplish these objectives, we utilized robust and comprehensive, spatiotemporal river discharge estimates described by (Shope et al., 2013) at 14 locations throughout the Haean catchment to quantify flow partitioning. We discuss the construction of the ecohydrologic SWAT model for the Haean catchment, the selection and sensitivity of model parameters, and the calibration and validation of the model. Finally, we evaluate three different river routing systems including, (1) the surface water drainages, (2) a combination of the rivers and engineered culverts, and (3) the rivers, culverts, and road network, to identify flow partitioning throughout the catchment.

## 2 Catchment characteristics

### 2.1 Location and physiography

The Haean catchment study area (38.239–38.329° N; 128.083–128.173° E) is located in the Gangwon Province of the northeastern portion of South Korea along the demilitarized zone (DMZ) between South and North Korea (Fig. 1). The 62.7 km$^2$ catchment has a unique bowl-shaped physiographic characteristic, which drastically alters the local meteorological conditions. Elevation ranges between 339 to 1321 m a.s.l. with an average slope of 28.4 % and maximum slope of 84 %. The catchment drainage is the Mandae Stream with a maximum length of 8.6 km. Limited historical observations are available, although this is typical for most areas outside of Europe and North America.





HESSD
10, 7235–7290, 2013



## 2.2 Haean climate

The climate in South Korea is humid continental to humid subtropical, influenced by the East Asian summer monsoon and early autumn typhoons that bring strong winds and heavy rains. Precipitation is concentrated in the short, persistent, intense, monsoonal rainy season called *Changma*. The monsoon season extends from the end of June through the end of July, followed by scattered events through early September, with up to 70 % of the total annual precipitation between the months of June and August. The average annual rainfall over the most recent 12 yr of record is 1514 mm (930 to 2299 mm $yr^{-1}$) with a maximum precipitation as high as 48.6 mm $h^{-1}$ or up to 223.2 mm $d^{-1}$. The average annual temperature is $8.65 \pm 0.35$ °C ranging between −26.9 °C in January to 33.4 °C in August. The average catchment discharge at the outlet is 37 $m^3 s^{-1}$ with an observed maximum of 258 $m^3 s^{-1}$ in August 2010 and baseflow discharge rates typically near 3 $m^3 s^{-1}$. The catchment hydrology is further described in Shope et al. (2013).

## 2.3 Catchment geology

Geologically, the basin is composed of a Precambrian gneiss complex at the higher elevation mountain ridges and a highly weathered Jurassic biotite granite intrusion that was subsequently eroded throughout the central portion of the catchment (Kwon et al., 1990). Alluvium generally extends up to 2 m in depth and bedrock is typically observed between 20 and 45 m below land surface in the catchment interior. Surficial soil texture is typically saprolitic sand and sandy loam with high infiltration capacity (Arnhold et al., 2013; Jo and Park, 2010).





HESSD
10, 7235–7290, 2013



## 3 Materials, methods, and model construction

### 3.1 Conceptual hydrology and mathematical approach

The SWAT model is a continuous, physically based, distributed model originally developed to predict the long-term impact of climate and land use management practices on hydrologic, sediment, and agricultural chemical yields in large, complex basins (Arnold et al., 1998). The model provides spatial discretization flexibility for detailed plot-scale assessment to regional-scale applications (Neitsch et al., 2010, 2011; Schuol et al., 2008a, b) and has been widely applied and validated throughout the world (Gassman et al., 2007). The GIS based ArcSWAT interface (Winchell et al., 2010) was utilized for model parameterization. During model construction, the catchment was divided, typically on a topographic basis, into spatially linked subbasins that represent the large-scale spatial heterogeneity used to accommodate water balance accounting. The subbasins were segregated into unique Hydrological Response Units (HRUs) by integrating the combination of land use, soil type, and slope to describe the system physical heterogeneity. Essentially, SWAT uses the water balance approach to simulate watershed hydrologic partitioning, where

$$\mathrm{SW}_t = \mathrm{SW}_o + \sum_{i=1}^{t} \left(R_{\mathrm{day}} - Q_{\mathrm{surf}} - E_{\mathrm{a}} - w_{\mathrm{seep}} - Q_{\mathrm{GW}}\right). \quad (1)$$

In Eq. (1), $\mathrm{SW}_t$ is the final soil water content (mm $H_2O$), $\mathrm{SW}_o$ is the initial soil water content on day $i$ (mm $H_2O$), $t$ is time (days), $R_{\mathrm{day}}$ is the amount of precipitation on day $i$ (mm $H_2O$), $Q_{\mathrm{surf}}$ is the amount of surface runoff on day $i$ (mm $H_2O$), $E_{\mathrm{a}}$ is the amount of evapotranspiration on day (mm $H_2O$), $w_{\mathrm{seep}}$ is the amount of water entering the vadose zone from the soil profile on day $i$ (mm $H_2O$), and $Q_{\mathrm{GW}}$ is the amount of return flow on day $i$ (mm $H_2O$) (Neitsch et al., 2010).

The modeled hydrological components are comprised of surface runoff, percolation, lateral flow, groundwater flow, evapotranspiration, and transmission losses. The





HESSD
10, 7235–7290, 2013



simulation of watershed hydrology with SWAT is split into the land phase of the hydrologic cycle controlling the amount of water, sediment, and nutrients into the main channel in each subbasin, and the channel or routing phase of the hydrologic cycle defined as the movement of water, sediment, and nutrients through the channel network to the watershed outlet (Neitsch et al., 2011). Incoming precipitation is partitioned into canopy storage, infiltration, and surface runoff through either the SCS (Soil Conservation Service) curve number (CN) method (U.S.D.A., 1972) or the Green-Ampt (Green and Ampt, 1912) method. Daily runoff volume from the SCS retention parameter can be calculated through the shallow soil water content or through accumulated plant evapotranspiration. The SCS curve number method with soil water content calculated runoff was selected for this study. The hydrologic condition of the vegetation is important in determining CN for individual HRUs (U.S.D.A., 1972). Therefore, the distributed CN was further modified within individual HRUs through time-variable land use characterization and crop growth. The model uses the modified Rational Method to estimate peak flow (Neitsch et al., 2011). Runoff is aggregated from the HRU level into the subbasin level and then routed through the stream network. The Manning equation is used to estimate the flow rate and velocity through the channels. Flow routing is based on either the variable storage or the Muskingum routing method; and for this study, we chose the variable storage method (Neitsch et al., 2011).

## 3.2 Hydrometeorologic data

### 3.2.1 Climate data

Hourly climate data for the period from 1998 to 2011 were measured and collected from several regional stations of the Korean Meteorological Agency (KMA) (Fig. 1). Precipitation and minimum/maximum temperature were obtained from the Haean KMA station in the center of the catchment (38.287° N, 128.148° E). Relative humidity, temperature, and wind speed were obtained from the Inje KMA station in the adjacent Yanggu County (38.207° N, 128.017° E). Solar radiation was collected from the Chuncheon





HESSD
10, 7235–7290, 2013



KMA station (37.904° N, 127.749° E). Distributed climate data were collected from 15 micro-meteorological stations (Delta-T Devices, Ltd.) throughout the catchment (Fig. 1) between 2009 and 2011. Sub-hourly data was aggregated into hourly precipitation (±0.2 mm), minimum/maximum air temperature (±0.2 °C), wind speed (±0.1 m $s^{-1}$), solar radiation (±5 W $m^{-2}$), and relative humidity (±2 %). The data were quality-controlled by first removing erroneous data and subsequently gap filling the missing data from a similar station using a weighted algorithm based on elevation, station proximity, and aspect. The algorithm as formulated for precipitation is presented as

$$P_e(z,d,\varphi) = \left\{ \begin{array}{l} \left[\sum_{i=1}^{a} \left(P_o\left[\text{minimize}_{i=1}^{v}(\varphi_e - \varphi_o)\right]\right) w_3\right] + \ldots \\ \left[\left(\sum_{i=1}^{a}\left[\left(\frac{d_x}{d_x+d_y}\right) * \left|P_x - P_y\right|\right] + P_x\right) w_2\right] + \ldots \\ \left[\sum_{i=1}^{a} \left(P_o\left[\text{minimize}_{i=1}^{v}(z_e - z_o)\right]\right) w_1\right] \end{array} \right\}. \quad (2)$$

The variable $P_e$ is the estimated precipitation (mm), $z$ is the elevation (m), $d$ is the distance to the observation point (m), $p$ is the observation point aspect (deg.), $i$ is the timestep, $a$ is the total number of consecutive missing data, $P_o$ is the observed precipitation (mm), $v$ is the total number of observational meteorological stations, $w$ is the weighting factor, and $x$ and $y$ are the first and second most proximal locations to the estimation location, respectively. The locally based relative humidity was modified by accounting for the temperature dependent local dew point. The SWAT model does not explicitly interpolate spatial meteorological conditions but instead, prescribes the meteorological parameter of the nearest weather station to the centroid of each subbasin for individual timesteps (Neitsch et al., 2011). Due to the large variation in elevation and topographical complexity throughout the catchment, significant meteorological impacts were expected to influence not only precipitation volume and soil moisture, but also plant growth. Therefore, we used an inverse distance weighted (IDW) interpolation method to grid the measured meteorological results throughout the catchment and added the virtual weather at each corresponding subbasin centroid. Principle data sources used for the Haean catchment ecohydrologic model are provided in Table 1.





HESSD
10, 7235–7290, 2013



### 3.2.2 Discharge and evapotranspiration measurements

Surface water discharge measurements were collected at up to 14 locations throughout the catchment between 2003 and 2011 (Fig. 1) as described by Shope et al. (2013). Both event-based and baseflow estimates were obtained through multiple methods including, the in-stream velocity-area technique (Rantz, 1982); multiple 90° V-notch weirs, acoustic Doppler current profiler (ADCP), solute dilution gauging, velocity derived estimates, volumetric methods, Manning equation calculations, and differential discharge gauging. Briefly, (Shope et al., 2013) found that each method displayed optimal precision over specific, although overlapping river discharge ranges.

The SWAT model also includes several methods to calculate potential evapotranspiration (PET) (Hargreaves and Samani, 1985; Monteith, 1965; Penman, 1948; Priestley and Taylor, 1972) depending on the observational meteorological data available. In addition, a single pre-calculated PET data set can be incorporated into the model. However, because of the robust and high frequency spatially variable micrometeorologic data available through the TERRECO project, we simulated daily PET using the Penman-Monteith method (Penman, 1948). As described in Ruidisch et al. (2013) and Shope et al. (2013), the weather conditions throughout the catchment are heterogeneous and therefore, the physically-based Penman-Monteith estimates were preferred over the alternative Priestly-Taylor or Hargreaves methods. Soil evaporation and crop transpiration were estimated using the FAO Penman-Monteith equation as described in Allen et al. (1988).

## 3.3 Spatial data

### 3.3.1 DEM

The Soyang watershed 30 m resolution digital elevation model (DEM) obtained from the National Geographic Information Institute (NGII) was clipped to the extent of the Haean catchment boundaries (Fig. 1). The DEM was used to define subwatershed





HESSD
10, 7235–7290, 2013



boundaries, form slope classes, and determine channel characteristics throughout the catchment. The observed river network was geo-referenced and explicitly incorporated into the DEM because the modification of stream channels is reasonable in highly managed catchments similar to Haean and inclusion of stream delineation improves hydrologic segmentation and boundary delineation. In addition, extensive ground-based surveys of engineered channels, diversions, culverts, drainage features, sediment retention ponds, and roads throughout the Haean catchment were completed. To investigate the role that engineered structures have in channel routing, three channel classifications were constructed for (1) the river network, (2) the river network and engineered culverts, and (3) the river network, culvert system, and existing roads (Fig. 2). The Haean catchment was divided into three slope classes representing steep forested high elevation (10° to 90°), moderately sloped dryland agriculture (2° to 10°), and mildly sloping rice paddies in the central portion of the catchment (0° to 2°) (Table 2).

### 3.3.2 Soils

Regional soil information was obtained from the Rural Development Administration (1 : 25 000) and based on a single surficial soil layer. The Haean spatial soil dataset (TERRECO) coupled the RDA regional soil data, agricultural land use classifications, and extensive field-based soil profiles to develop a spatial distribution of multiple soil horizons to a depth of 3 m. Our results found that Haean soils are intensively managed and modified and depend on land use more than the specified soil type (Tenhunen et al., 2011). Soil properties, including the hydrologic soil group, texture class, the percentage content of rock, sand, silt, and clay content, and the hydraulic conductivity, were derived from an extensive 2009 catchment-wide field survey that was aggregated into 6 unique soil types (Table 2).





HESSD
10, 7235–7290, 2013



### 3.3.3 Land use and land cover

Intensive field-based, plot-scale land use/land cover (LULC) observations for each of the years 2009 through 2011, resulted in up to 126 individual LULC classes. For the purposes of this study, the 2009 ground survey data have been distilled to 15 different LULC classes (Table 2). Haean is a mixed land use catchment, which contains 54 % agricultural land, where agricultural fields are typically less than 0.40 $km^2$. The remainder of the catchment area is upland forest at higher elevations, predominately composed of 30 to 40 yr old mixed deciduous forest. Major species include Mongolian oak (*Quercus mongolica*), Daimyo oak (*Quercus dentata*), and Korean ash (*Fraxinus rhynchophylla*).While this highly agriculture dependent catchment has exhibited variations in LULC distribution and increasing forested encroachment (Kim et al., 2011), the LULC distribution throughout the study period between 2009 and 2011 remained relatively stable (±1.2 %, Yanggu County Office, 2012).

## 3.4 Management inputs and crop parameterization

### 3.4.1 Management parameter estimation

Agricultural management practices within the Haean catchment were surveyed between 2009 through 2011 through a combination of on-site stakeholder interviews, empirical field observations (Tenhunen et al., 2011), published literature (i.e., Nguyen et al., 2012), and regulatory reports from the Research Institute of Gangwon (RIG), the Ministry of Environment, the National Institute of Agricultural, Science, and Technology, and the Korean Forest Research Institute. To develop a comprehensive analysis of field-based crop management activities, more than 300 interviews of stakeholders and farmers were completed under the TERRECO project to quantify fertilization and pesticide application quantities and timing, irrigation practices, planting and harvesting activities, tillage methodologies, and additional demographic and sociological information (Poppenborg et al., 2013; Trabert et al., 2013; Nguyen et al., 2013). In addition,





HESSD
10, 7235–7290, 2013



student-managed TERRECO harvest plots were used to obtain a comprehensive observational analysis of temperature-based planting, fertilizer, tillage, mulching, development, and harvest procedures (Tenhunen, unpublished data). An example of the land use and crop management schedule, application rate, and application frequency is provided in Table 3. Parameters within the SWAT database consistent with fertilizer applications were varied for each crop and subbasin to allow for spatially distributed management applications and the influence of meteorological drivers. The simulated timing of management actions (i.e., fertilization, tillage, planting, irrigation, harvesting) were implemented in SWAT through daily heat unit summations rather than explicitly defining the Julian day because traditional planting and harvest methods are dependent on climatic observations closely correlated to heat units (Shope et al., 2013).

### 3.4.2 Biomass sampling, analysis, and plant growth

Biomass analysis was completed by collecting and sampling 5 to 10 entire plants, representative of each crop type (Table 2) from a 2009 catchment-wide sampling campaign of student-managed TERRECO harvest plots (Tenhunen, unpublished data). Each of the plants was field separated into fresh leaves (green), decay material (brown), stems, and roots and subsequently weighed for fresh weight. The leaf area was individually measured using a portable leaf area meter (Opti-Sciences, Inc., AM 300). The samples were subsequently separated and dried at 80 °C for more than 1 week, prior to measuring the sample dry weight.

To differentiate between crop types particular to South Korea (i.e., ginseng), several modified land use classes were created in the SWAT crop database. Nine observed field plots representing the major crop types and forest along an elevation transect were analyzed and crop parameters were varied to minimize the simulated and observed residuals for leaf area index (LAI), biomass, and crop yield. The crop parameters were altered based on observed measurements, plant physiology modeling results (PIXGRO), published literature, regulatory reports, and stakeholder input. The crop parameters that were varied are presented in Tables 3 and 4. Intensive cultivation was also





HESSD
10, 7235–7290, 2013



present in agricultural areas not serviced by irrigation canals and therefore, groundwater abstraction was estimated from the PIXGRO model as the quantity required for optimal plant growth. Typical to many Asian catchments, Haean can be considered a highly managed catchment with increased uncertainty due to insufficient spatiotemporal water management data.

### 3.4.3 Rice paddies, potholes, and water abstraction

The quantity and timing of river and groundwater abstractions is uncontrolled and local estimates were inadequate for model inclusion. Depending on the HRU location, irrigation water was extracted from an adjacent river reach or from deep groundwater. Groundwater-derived irrigation practices were limited to orchards and rice paddies and were accounted for in the simulations through water availability based auto-irrigation at the HRU level and defined by the soil water deficit. Rice paddies were simulated in SWAT as potholes, which are hydrologically similar to ponded areas. Rice paddies are typically characterized by multiple cascading-elevation plots separated by embankments that retain surficial water storage prior to channel routing. The rice paddies had low infiltration and typically saturated soil conditions and therefore, infiltration as a function of water content rather than flow routing was used for estimation of losses to the subsurface. The HRUs within each subbasin were developed using 0 % land use and 0 % soil threshold for reach subbasins resulting in maximum number of HRUs. A 51 % soil threshold was prescribed to create a single rice paddy HRU from the original multiple land use HRU distribution in order to characterize the rice paddy HRU as a single pothole.





HESSD
10, 7235–7290, 2013



## 4 Results and discussion

### 4.1 Meteorological drivers and the effects of interpolation

Meteorological time series data, particularly precipitation is a highly sensitive driver in hydrologic modeling applications. Spatial monitoring distributions are typically limited and do not capture heterogeneous meteorological conditions that can be interpolated by wide-meshed monitoring networks (Notter et al., 2007). As described, large variations in elevation and topographical complexity throughout the catchment influence the precipitation volume, soil moisture, and plant growth. They can also influence the peak flow and the time of concentration to peak discharge of the simulated hydrograph (Khakbaz et al., 2012; Wilson et al., 1979). Our weather analysis revealed heterogeneous meteorological conditions throughout the Haean catchment (i.e., Choi et al., 2010; Shope et al., 2013). To summarize, hourly precipitation and solar radiation was extremely variable and in large part, focused in individual subregions and dependent on elevation and aspect. These variations in precipitation and solar radiation have a direct influence on the relative humidity and therefore, the spatial influences on plant growth parameters indicate a significant variability between subbasins in the Haean catchment (Fig. 3).

We assessed the effect of subbasin size and HRU definition on surface water discharge and found no appreciable difference between model results. However, care must be taken for subbasins with steep slopes and extensive vertical gradients to account for elevation based climate conditions, which contribute to highly variable ET conditions. Choi et al. (2010) found that the temperature lapse rate within the Haean catchment ranged between $-0.56\,^{\circ}\mathrm{C}\,100\,\mathrm{m}^{-1}$ throughout the spring to $-0.27\,^{\circ}\mathrm{C}\,100\,\mathrm{m}^{-1}$ on cloudy winter days. Temperature inversions as high as $+1.0\,^{\circ}\mathrm{C}\,100\,\mathrm{m}^{-1}$ were observed during early morning hours after many consecutive sunny days. These results imply that stagnant East Asian monsoon high pressure systems can significantly vary climatic conditions on a local scale. Therefore, a temperature lapse rate of $-0.52\,^{\circ}\mathrm{C}\,100\,\mathrm{m}^{-1}$





HESSD
10, 7235–7290, 2013



was incorporated into the continuous spatial interpolation for temperature boundary conditions.

We examined the model sensitivity to alternative precipitation interpolation methods (IDW, Spline, nearest neighbor, and Kriging), both through spatially explicit plant growth response and river discharge to assess the robustness of interpolation in our domain. We found that total river discharge between interpolation methods varied less than 0.1 % at the integrated catchment outlet (S7) and the discharge differences at multiple locations throughout the catchment (S1, S4, S5, and S6) were negligible. The IDW univariate interpolation technique for precipitation did result in slightly improved plant growth response for selected crops and locations than other methods. Similar to results obtained by Notter et al. (2012), the IDW method was invoked to develop a continuous grid of meteorological drivers that were subsequently assigned to individual subbasins.

### 4.2 Model calibration, validation, and uncertainty assessment

#### 4.2.1 Sensitivity and model parameterization

Strategies to parameterize distributed models typically involve reducing the dimensionality of the calibration problem and solving it through optimization algorithms. A substantial reduction in the number of calibration parameters can be accomplished by describing the spatial variability within an HRU in terms of probability distributions. While a global sensitivity analysis provides insight into the mathematical model and the behavior of the conceptual watershed, a more robust approach is to analyze the differences in model sensitivity at multiple locations. The purpose of this is to quantify spatial variability in the observational sensitivities and parameterize accordingly. This enabled us to define scale-dependent model parameters for increasing drainage area contributions. The sensitivity analysis of discharge related model parameters was achieved by sequentially varying an individual parameter while maintaining the remaining parameters for each monitoring location. Between eight and eleven parameters from the original 15 discharge-related parameters were found to be sensitive to catchment-wide flow





HESSD
10, 7235–7290, 2013



partitioning (Fig. 4). Subsequently, the range of each of the parameters was adjusted during calibration procedures.

The use of lumped, semi-distributed, and fully distributed model parameterization was also investigated through sensitivity analysis. We assigned the same parameter magnitudes by crop type for the lumped distributed parameters. The parameters were assigned by crop type and varied by subbasin location for the semi-distributed model construction. We varied parameters by individual HRU locations for each of the crop types in the fully distributed construction. We found that fully distributed parameters between subbasin, soil, and land use classifications were negligibly better than semi-distributed parameters based on aggregated land use classifications within individual subbasins. We also found that the use of a lumped parameter assignment did not perform as well as either the fully- or semi-distributed parameterization. Therefore, for computational efficiency, a semi-distributed approach was taken throughout the catchment utilizing the most sensitive parameters at each monitoring location for parameterization in adjacent areas. While we did not explicitly quantify the optimal parameterization, through a series of iterations we weighted the objective functions ($R^2$, NSE, PBIAS, and baseflow percentage) in decreasing order as we compared individual locations throughout the catchment. In effect, we used a multi-criteria decision making process with the goal of determining the relative total priority of each alternative when all of the criteria were considered simultaneously. Because our results indicated that the sensitivity analysis was significantly based on the monitoring location, we calibrated multiple locations along an elevation transect. In Fig. 4, the *t* stat provides a measure of parameter sensitivity where larger absolute values are more sensitive (Abbaspour, 2011). The *p* value determines the significance of sensitivity with higher significance as values approach zero (Abbaspour, 2011). Results generally indicate surface runoff and routing parameters are more sensitive at higher elevations with increasing sensitivity to infiltration and groundwater parameters at lower elevations (Fig. 4). The REVAPMN groundwater parameter was a sensitive parameter at each location; however, the magnitude was relatively small. CH_K2 was the least sensitive parameter, although included





HESSD
10, 7235–7290, 2013



in the analysis for comparison. The infiltration parameters suggest significant baseflow response at higher elevations. At mid-elevations, surface runoff and routing parameters become more sensitive. At lower catchment elevations, infiltration, routing, and groundwater parameters dominate. These results identify the importance of and differences between model sensitivities as a function of the inherent mathematical equations and the model sensitivity as a function of observational dynamics. Therefore, caution should be exercised in rainfall-runoff process simulations in relatively ungauged basins.

#### 4.2.2 Metrics of model performance for calibration procedures

Model performance was assessed by several metrics at each location including; the simulated and observed water balance, the coefficient of determination ($R^2$), Nash Sutcliffe Efficiency (NSE), percentage bias (PBIAS), and the baseflow contribution. The $R^2$ was used to assess whether the simulations reproduced observed variability of natural hydrologic processes while minimizing the overall residuals. The $R^2$ ranges between 0 and 1, with higher values indicating less variance and is calculated as

$$R^2 = \frac{\left[\sum_{i=1}^{n}\left(Q_{\text{obs}} - \overline{Q_{\text{obs}}}\right)\left(Q_{\text{sim}} - \overline{Q_{\text{sim}}}\right)\right]^2}{\sum_{i=1}^{n}\left(Q_{\text{obs}} - \overline{Q_{\text{obs}}}\right)^2 \sum_{i=1}^{n}\left(Q_{\text{sim}} - \overline{Q_{\text{sim}}}\right)^2} \quad (3)$$

where, $Q_{\text{obs}}$ is the observed stream flow, $Q_{\text{sim}}$ is the simulated streamflow, and $\overline{Q_{\text{obs}}}$ and $\overline{Q_{\text{sim}}}$ are the average observed and simulated streamflow throughout the modeled period. The Nash-Sutcliffe efficiency (NSE) is a normalized correlation related statistic used to compare observational variance to the residual variance, particularly during peak events (Nash and Sutcliffe, 1970). The NSE ranges between $-\infty$ and 1, with optimal values approximating 1. The NSE is calculated as





HESSD
10, 7235–7290, 2013



$$\mathrm{NSE} = 1 - \left[ \frac{\sum_{i=1}^{n} (Q_{\mathrm{obs}} - Q_{\mathrm{sim}})^2}{\sum_{i=1}^{n} \left(Q_{\mathrm{obs}} - \overline{Q_{\mathrm{obs}}}\right)^2} \right]. \quad (4)$$

As Moriasi et al. (2007) describes, NSE values between 50 and 65 may be considered satisfactory, between 65 and 75 are considered good, and very good results are from 75 to 100. The percentage bias (PBIAS) is a quantitative measure of simulated versus observed river discharge for the entire simulation period and defines the total volume differences between the simulated and observed fluxes as calculated by

$$\mathrm{PBIAS} = \left[ \frac{\sum_{i=1}^{n} (Q_{\mathrm{obs}} - Q_{\mathrm{sim}}) \times 100}{\sum_{i=1}^{n} Q_{\mathrm{obs}}} \right]. \quad (5)$$

Positive values indicate that the model underestimates observed results and negative values indicate model overestimation. Therefore, PBIAS should be near zero (Gupta et al., 1999). PBIAS values between 15 and 25 are considered satisfactory, between 10 and 15 are considered good, and values less than 10 are considered very good (Moriasi et al., 2007).

#### 4.2.3 Manual and automated model calibration

The model sensitivity was addressed with respect to spatial distribution (number and location of meteorological stations, LULC distribution), observational record (LULC coverages, meteorological stations), resolution (soil coverage, subbasin discretization), and hydrologic stimulus (rainfall-runoff). The Haean catchment model configuration resulted in 142 topographically based subbasins and 2532 individual HRUs. Previous investigations have shown that the number of subbasins has little influence on runoff (Jha et al., 2004; Tripathi et al., 2006; Xu et al., 2012a, b). However, our results show that elevation-based plant parameters and convective precipitation captured through





HESSD
10, 7235–7290, 2013



increased subbasin discretization can be important and therefore 13 subbasins with high elevation ranges were subdivided.

The Haean ecohydrologic SWAT model was simulated from 2006 through 2011 with the first 3 yr excluded for model initialization during the calibration period. For this study, the calibration and validation of the spatially variable river discharge was carried out in a daily timestep using river discharge data from the hydrologic years 2009 through 2011. The model was calibrated to the 2010 field data and validated against a combination of 2003, 2004, and 2009 discharge estimates for each of the 14 monitoring locations. Calibration of watershed models is often achieved using inverse modeling methods (i.e., Kunstmann et al., 2006). The primary goal of inverse modeling is to characterize model parameterization primarily through assigning parameter distributions associated with parameter uncertainties (Abbaspour et al., 2004). Observed streamflow at both selected interior locations within the catchment (S1, S4, S5, and S6) and the catchment outlet (S7) were utilized for daily and monthly model calibration to better parameterize spatial variability in hydrologic partitioning. These monitoring locations are distributed throughout the catchment along an elevation gradient and therefore, provide regional representation of model parameterization. In addition, the unique punchbowl shape enabled the calibration parameters to be correlated to other ungauged subcatchments with similar slope and elevation.

Model calibration was separated into two major components, (1) manual catchment scale calibration to estimate system processes and variability, and (2) automated calibration to quantify model uncertainty. Initially, the entire catchment was calibrated at the catchment outlet (monitoring location S7) and then individual locations within the catchment were subsequently calibrated beginning with the highest elevation locations and ending with a final calibration at the catchment outlet. The observational data for individual stations were not always collected over the entire simulation period and therefore, different validation periods were used. For example, location S4 was calibrated to the 2010 observational data, although there was limited data to validate for 2009. Therefore, with respect to similar topography, elevation, and land use patterning, SD





HESSD
10, 7235–7290, 2013



was used to validate the S4 calibration results. Intensive manual calibration was performed at each of the subbasins routed to a monitoring station by individually varying the sensitive parameters. Although, the manual calibration results were used to minimize the acceptable parameter range at each site and assess the parameter impact on the simulated river discharge. The difficulty is that manual calibration sensitivity suffers from the linearity assumption by not accounting for correlations between individual parameters.

After manual calibration was sufficient, automated model calibration, validation, and uncertainty analysis were completed using the Sequential Uncertainty Fitting Algorithm (SUFI-2) (Abbaspour et al., 2004, 2007). Uncertainties within the conceptual model, data inputs, and individual parameter selection are aggregated using SUFI-2 with the objective of obtaining the minimum range in uncertainty while bracketing the majority of the data (Schuol et al., 2008a). The described manual calibration results provided distributed, physically based parameter ranges that were subsequently incorporated into the SUFI-2 auto-calibration routine, starting with the catchment outlet and following a top to bottom approach. Throughout the SUFI-2 optimization process, the parameter ranges were iteratively decreased by combining a random search procedure and complex parameter iteration algorithm to direct the parameter space and global optimization (Abbaspour et al., 2004). Model uncertainty is subsequently quantified by the 95 % prediction uncertainty (95PPU) at the 2.5 % and 97.5 % cumulative distribution, which is obtained through Latin hypercube sampling procedure (Abbaspour et al., 2004). Because the model efficiently varies multiple parameters at the same time, two indices are used to assess the stochastic calibration performance. The *p* factor describes the percentage of data bracketed by the 95 % prediction uncertainty and should be as large as possible up to a maximum value of 100. The *r* factor describes the average width of the prediction band divided by the standard deviation of the measured data, which represents the range of the uncertainty interval and should be minimized, approaching zero (Faramarzi et al., 2009). Since the uncertainty in field-based river discharge measurements was typically $< 5$ % (Shope et al., 2013), a conservative 10 %





HESSD
10, 7235–7290, 2013



measurement error was included in the $p$ and $r$ factor calculations (Abbaspour et al., 2009; Andersson et al., 2009; Butts et al., 2004; Schuol et al., 2008a). Yang et al. (2008) found that reasonable prediction uncertainty ranges were achieved with 1500 repeated model simulations. Further, Güngör and Göncü (2013) specifically showed that 300 iterations provided similar results to 1500 iterations. Therefore, at least 300 iterations of all simulations at each location were performed throughout the auto-calibration routine (Table 5).

As described, the calibration parameters were selected to optimize the PBIAS, $R^2$, and NSE test statistics and the contribution of groundwater baseflow estimated from the hydrograph analysis. The main SWAT parameters controlling baseflow processes in Haean include GWREVAP, GWQMN, GWDELAY, ALPHABF, and ESCO. The primary parameters that affected surface runoff throughout the Haean catchment are CN2 and SOLAWC. During model calibration procedures, the ESCO and GWREVAP parameters were typically adjusted to minimize the PBIAS and improve the yearly river discharge and water balance trends. The GWQMN parameter was then adjusted to simulate the seasonal discharge trends that were assessed through the monthly NSE statistic. Finally, the CN2, CH_N2, and GWDELAY parameters were calibrated to account for daily trends by minimizing the NSE. Our results also indicated that the NSE increased by changing the stream routing method from variable storage to Muskingum routing. When the Muskingum method was utilized, the channel parameters CH_N2 and CH_K2 were ranked 2 and 3 in the sensitivity analysis. However, the relative change in NSE between outlet results was negligible ($\sim 0.01$) compared to the default variable storage routing method, and the addition of more parameters was substantial. Therefore, variable storage routing within the SWAT model was chosen to limit the model parameterization.

The explanation for the deviations in runoff at the low elevation locations (S6 and S7) is not known or reflected in the SWAT input data. However, by examining a combination of optimized calibrated data, process-based comparisons, and field observations, the overall calibration metrics indicated increased flow routing directly from high elevation locations to lower elevation river locations. A possible explanation is the density of





HESSD
10, 7235–7290, 2013



surface water collection and sedimentation ponds within the catchment, which may have impacted the observed runoff characteristics of the watershed (Cho et al., 2012). Using a multi-criteria optimization approach, we identified that engineered flow routing and infrastructure construction such as roads and culverts, contributed to increased discharge at lower elevations. These catchment-wide landscape engineering results are further discussed in Sects. 5.4 and 5.7.

### 4.3 Spatiotemporal flow partitioning with respect to river discharge

The calibration and validation of the Haean catchment daily discharge yielded good results given the scarcity and the temporal longevity of some of the available data. The modeling results indicated that SWAT performance at the Haean catchment relied heavily on the quality and more importantly abundance of discharge data, similar to the results of Dessu and Melese (2012). The NSE score for monitoring locations S1, S4, S5, S6, and S7 ranged between 0.64 and 0.95 with an average score of 0.76 for the 2010 calibration period and between 0.40 and 0.98 for the validation period (Fig. 5). Satisfactory NSE scores of $>0.5$ were achieved at all 14 gauge locations in the calibration period and at 12 of 14 in the validation period. The $R^2$ value was also reasonable for each of the monitoring locations, ranging from 0.70 to 0.96 with an average value of 0.81 for the calibration period and between 0.71 and 0.97 for the validation period (Fig. 5). The fact that similar performance measures were reached in the validation as in the calibration period indicates that there was minimal "overfitting" of the distributed parameters.

The baseflow contribution estimated at monitoring location S4 using a digital filter hydrograph separation technique was 26 % (Shope et al., 2013), although the calibrated estimate was 42 %. The hydrograph separation magnitude varied significantly, depending on the data quality, the length of the analysis, and the timestep investigated (Shope et al., 2013). However, the digital filter methodology for estimation of the hydrograph separation is not process-based and may provide a significant deviation in accurate magnitude. The calibrated amount of 42 % at SW4 is similar to the estimates





HESSD
10, 7235–7290, 2013



at the upstream location S1, and therefore the variability in quantifying the shorter time period may indicate that the value is still within the estimate uncertainty.

We also observed increased differences between simulated and observed discharge estimates or water balance as measured through the PBIAS statistic at locations S6 and S7, which were 41 and 29 %, respectively. These PBIAS estimates are considered unsatisfactory according to Morasi et al. (2007), regardless of the very good metrics predicted through the $R^2$ and NSE statistics and the acceptable estimate of baseflow contribution. The increase in water balance was hypothesized to be a function of rapid and large flow contributions from high elevation locations that were routed through culverts, drainages, and road systems to lower catchment locations. The runoff was anthropogenically routed to the rivers and not infiltrated throughout the landscape. Essentially, the effect of the routing downstream not only creates a large disparity in simulated discharge, but limits the subsurface infiltration at the plot-scale for higher elevation locations and surreptitiously develops a misleading flashy flow system with reduced landscape water storage.

The lower NSE score and $R^2$ values could be attributed to the low relative variability of discharge at higher elevation monitoring locations, which contributes to increased deviations of NSE scores during event conditions, particularly monsoonal extreme events. At monitoring location S1 and SK, the NSE score was low, primarily due to several factors. Because the river discharge at these monitoring locations is lower, the relative observational error and measurement uncertainty is increased. At location SK, there is significantly decreased observation data and because the NSE statistic in particular weights the extreme events higher, limited although higher deviations have a much larger impact than minor deviations. In addition, the difficulty in accurately simulating the river discharge at monitoring location SK was hypothesized to be a function of high elevation flow contributions that bypassed the monitoring gage as hyporheic flow (Shope et al., 2013). The hydrological response throughout East Asia and within the Haean catchment in particular, was observed to be flashy and erratic, further attributing to event-based deviations in the objective functions. At monitoring location S5,





HESSD
10, 7235–7290, 2013



a higher temporal density of observations was obtained and the model performance is generally better than in other locations for both calibration and validation periods.

Overall, the calibration and validation results were good and the percentage of baseflow contribution at each location was reasonable in terms of the hydrograph separation estimates. The auto calibration metrics of $p$ value and $r$ value are both reasonable, while the $R^2$ and NSE statistics were consistently above satisfactory and predominately considered very good. The average $p$ factor throughout the calibration period at all stations was 65 % (0.54 to 0.69 %) and the $r$ factor was 0.21 (0.10 to 0.38 %). The average $p$ factor and $r$ factor from the validation period was 74 % (0.64 to 0.79 %) and 0.12 (0.10 to 0.21 %), respectively. This indicates that the majority of the simulated results were within the 95 % confidence interval and that the standard deviation was adequately minimized (Fig. 5). For locations, S4 and S6, we did not have observational records for the 2010 validation period and instead used the concept of self-similarity for validation results. Since the transect followed an elevation gradient in a limited portion of the catchment, we conceptualized that similar hydrologic processes were occurring for similar elevation and drainage areas in other parts of the catchment. Therefore, we used observational and simulated results from other parts of the catchment to compensate for locations with similar elevation, topography, drainage area, and land use distribution. As provide in Fig. 5 and Table 6, the validation results at these locations were good and consistent with the results estimated at other monitoring locations.

Each of the objective functions, hydrologic partitioning quantified by PBIAS, and the baseflow percentages were calibrated simultaneously, which while optimizing the values of some parameters, were at the detriment of other parameters. For example, at S5 the NSE was initially 0.89; however, parameter adjustments were made to minimize the water balance as PBIAS, which resulted in a lower NSE value. The event on 1 September 2009 displayed a substantial influence on the magnitude of the NSE and $R^2$ objective function. This is primarily due to the paucity of observation points and therefore, the weight of individual points, particularly during peak events, on the overall relationship.





HESSD
10, 7235–7290, 2013



The simulation results were very good in terms of adequately simulating baseflow contributions, the majority of moderate events, and most extreme events for each location. In addition, the other statistical objective functions were typically found to be good to very good and therefore, the balance in overall model simulation was found to outweigh individual discrepancies. It cannot be overstated that, the quality of input data, such as the estimated river discharge (Shope et al., 2013) or the short duration of observational data, was shown to significantly affect the model performance. For example, extensive observational data was collected at S5 although limited at S4 and S6, and the result is quantified by decreased statistics at the latter locations, even after extensive calibration. The relatively large 95 PPU band *r* factor necessary to bracket the observed data indicates that the uncertainty in the conceptual model is also very important for the Haean catchment.

### 4.4 Agricultural management and production

The heat sum methodology used to estimate time variable management and planting actions, provides the flexibility to account for unseasonable variations in meteorological drivers between years (Fig. 3). Heat sums are calculated as the cumulative temperature greater than the base temperature of 0.0 °C. The heat units are the cumulative heat sums initiated on the planting date and completed at the maximum growth. The HUSC is the percentage of the total heat units necessary for optimal growth of an individual crop and is prescribed for each management activity. The minimum heat sum over the period of record was 4246 °C during 2009, the maximum was 5783 °C during 2003, and the average annual heat sum is 5222 °C (Fig. 6). The 12 yr linear trendline of maximum cumulative annual heat sum values indicates a general decrease of nearly 0.2 °C per year. While precipitation trends suggest more extreme events occurring over a shorter time, these results indicate a decreasing trend in annual heat output necessary for optimal plant growth and therefore production.

To evaluate the SWAT simulation results on the ecohydrologic response, we also analyzed the simulation results in terms of agricultural growth dynamics at selected plot





HESSD
10, 7235–7290, 2013



locations throughout the catchment. While calibrating spatiotemporal discharge as previously described, we also investigated the effect of crop dynamics through temporal leaf area index (LAI) as a proxy for crop growth and development (Fig. 7). Individual crop growth and development parameters were adjusted for a comparison between observed and simulated LAI (Table 4). Results indicate a generally reasonable approximation of simulated LAI where the $R^2$ for each of the crop types ranged from 0.51 to 0.76 (Fig. 7). More importantly, the results provide a consistent estimate of temporal trends in simulated biomass or agricultural production under these hydrologic conditions for several major crops throughout the catchment.

The crops analyzed during the 2009 growing season account for 85 % of the total Haean land use. The remaining 9.5 % is divided into barren landscape and the negligible distribution of residential, water, orchard, ginseng, and other land use types. Rice accounts for 90 percent of the total Korean agricultural product and soybeans is the primary source of the Korean oilseed production. As provided in Table 7, when individual plot production is scaled to the catchment level, the Haean catchment is a productive agricultural system. Haean rice yield is more than 150 % of the national average, potato is slightly more than the national average, and soybean amounts to more than 8.5 times the national average. There was a slightly less estimate of cabbage yield and the radish yield in Haean was approximately 70 % of the national average. The reduced radish estimate may be a function of the particular plot and not necessarily representative of the average production in the Haean catchment. More importantly, while there is a greater percentage of the staple rice crop than the national average, the Haean catchment has experienced a shift to high value crops. This includes an increase, for example in radish and ginseng crops distributed throughout the catchment (Yanggu County Office, 2012).

### 4.5 Influence of engineered landscape structure

While both the calibration and validation indicate successful spatial results with very good metrics, a point of concern between observed and simulated results was at





HESSD
10, 7235–7290, 2013



monitoring locations S6 and S7. The river discharge discrepancies between simulated and observed results were realized through PBIAS, which essentially accounts for differences between the observed and model computed water balance. Consistent with field-based visual observations, catchment-wide surface runoff near the high elevation crops is routed to culverts immediately adjacent to the individual fields and road networks directly to the low elevation portions of the catchment. As indicated in Fig. 2, many of these long, extensive features traverse from high elevation plots near the forest boundary down to the lower portions of the catchment. Based in large part on a nationally subsidized federal aid project, the Haean roads and culverts were generally constructed approximately three years prior to the investigation, which provides an opportunity to see their effect on the system. Since the poured concrete culverts are immediately adjacent to many of the plots, decreased infiltration occurs in the agricultural areas and throughout the length of the culvert. This anthropogenic influence has the distinct disadvantage of reducing landscape-scale infiltration required to maintain local soil moisture storage, also in addition to rapidly transporting excessive nutrients from fertilizer applications into the lower parts of the catchment. This results in a rapid injection of elevated nutrient concentrations and sediment into the river discharge. Therefore, while there is a significant influence on landscape-scale surface runoff, river discharge, and effectively hydrologic partitioning, a potentially greater issue is the impact expected from the rapid and large-scale alteration in water quality.

To test the impact of these anthropogenic engineered structures on catchment-wide hydrologic partitioning, we compared several different surficial flow routing configurations. The routing configurations utilized in the model simulations were (1) with rivers only, (2) with both rivers and culverts, and (3) a combination of rivers, culverts, and roads (Fig. 2). As previously described in Sect. 5.3, the model performance in terms of PBIAS decreased toward the catchment outlet, particularly near S6 and S7. As the transect continues to the catchment outlet, the *p* factor decreases from 71 % to 11 %, suggesting that less data is bracketed by the 95 % confidence interval, while the *r*





HESSD
10, 7235–7290, 2013



factor describing the standard deviation of the observed discharge increases from 0.20 to 0.36.

When the model was reconfigured to account for both the river drainage network and the culverts, a better calibration was obtained where the PBIAS at monitoring locations S6 and S7 decreased from 41 and 29 % to 8 and 9 %, respectively. The dramatic difference in PBIAS was not extended by including the roads into the river and culvert drainage network. Our results indicated that a negligible increase in PBIAS was observed at both S6 and S7. Therefore, inclusion of the field-based drainage culverts was effective in moderating the difference in observed and model computed river discharge at lower elevation monitoring points; however, the benefit gained by adding the road system was negligible. The addition of culverts is consistent with field-based observations of event-peak flow routing through the Haean watershed. However, it is surprising that the road network had minimal influence. During peak event conditions, substantial overland flow and sediment transport was observed throughout the Haean catchment.

## 5 Summary and conclusions

We simulated spatiotemporal river discharge using a novel catchment-wide, multi-location, multi-objective function method, which increased the confidence of our results. Because the catchment is essentially a bowl-shaped topographic feature, the concept of symmetry enabled the results from a single elevation-based transect of monitoring locations to be utilized in catchment wide model calibration and validation. The computed discharge results were compared to observed discharge values and found to be good to very good under most circumstances, both during calibration and validation. Our goal of simulating high frequency monsoonal events in an area of complex physiographic topography provided substantial reliability in the use of the SWAT model in similar mountainous areas, particularly throughout East Asia. Our results show that fundamental shifts between surficial and baseflow driven hydrologic flow partitioning occur





HESSD
10, 7235–7290, 2013



within the catchment. High elevation steep sloping regions were found to be generally baseflow dominated while lower elevation locations were predominately influenced by surface runoff.

However, there were limitations in the reliability of modeling in similar regions, particularly in respect to field estimates, data collection, and the conceptual model. From the field perspective, some of the observed discharge measurements were performed approximately once per month during baseflow conditions and periodically throughout a monsoonal event on subdaily timesteps. In relatively ungauged locations, it can be difficult to adequately distribute a monitoring network with high frequency temporal resolution. In addition, data gaps were increased due to equipment malfunction and instrument sensitivity to ice. This is an expected and foreseeable result of multi-year investigations in seasonally snow covered regions. Another significant source of uncertainty was the irrigation and consumptive use water withdrawals; however, limited detailed data was available on the quantity, timing, or location of water withdraws and was incorporated into the model. The use of the SCS curve number methodology (U.S.D.A., 1972) is a relatively easy way to incorporate hydrologic conditions of a wide variety of behaviors. However, the method is controversial due to the empirical nature of the estimate and the daily method calculation rather than subdaily discretization (Lam et al., 2012). The model also relies on the HRU concept, which statistically averages subbasin processes and can limit the estimation of best management practices at the plot scale. Since it is a continuous time model with daily timesteps, subscale processes like event routing may not be efficiently and elaborately predicted (Lam et al., 2012). The SWAT model also estimates ET from daily averaged climate values rather than subdaily process-based estimates. To enhance the calibration of the SWAT model, we included plant growth as a simulation output. This methodology enabled us to compare simulated LAI to observed LAI and estimate plant growth rates and development to quantify biomass production as a function of land use.

The influences of engineered infrastructure systems (roads and culverts) were significant in hydrologic flow partitioning. Our results indicate that using multiple calibration





HESSD
10, 7235–7290, 2013



metrics and hydrologic characteristics ($R^2$, NSE, PBIAS, baseflow percentage, and plant growth) were influential in quantifying scale-dependent watershed processes. We used a unique combination of statistical, hydrologic, and plant growth metrics to calibrate our model, providing a robust and insightful characterization of catchment-wide hydrologic partitioning. By not including the culverts into the simulations, we demonstrate that the model simulations adequately represented observed spatiotemporal discharge but by including PBIAS as a calibration metric, we improved flow partitioning on the landscape scale by up to 33 %, particularly at the low elevation locations while minimal variations were observed at upper elevations. To optimize PBIAS, we explicitly included the culverts and the culverts and roads into the modeled drainage system to demonstrate that the spatially extensive irrigation culverts adjacent to most fields play an important role in flow routing. However, the addition of roads into the drainage system, minimally affected the simulation results. We observed in the field that both features played an important role in flow routing although it is likely that the roads ultimately returned overland runoff to the culvert drainage network or as subsurface infiltration.

To provide a higher accuracy estimate of spatiotemporal meteorological conditions, we used a unique high frequency, quality control, and gap-filling algorithm to develop a detailed interpolation of weather patterns. This provided a better estimate of the dynamic variability due to convective storm events. We demonstrate that the use of a multi-location, multi-objective function approach can drastically improve process-based estimates of catchment-wide hydrologic partitioning. Using a combination of statistical, hydrologic, and plant growth objective functions may provide a more comprehensive understanding of system interactions. By calibrating the model to many locations distributed throughout the catchment, landscape controls on hydrologic partitioning can be estimated as opposed to the integrated effect simulated at the catchment outlet. The results of this study elucidate the effect of catchment-scale engineered structures on discharge, nutrient loading, and contaminant transport. Care must be taken during model construction to avoid overlooking valuable hydrologic information and complex





HESSD
10, 7235–7290, 2013



relationships that may be deciphered through additional objective function metrics. This study also shows the challenges of applying the SWAT model to complex terrain and meteorological extreme environments. We successfully demonstrate that not only can the SWAT model be used in these locations, but that subdaily processes can be accurately simulated. However, care must be taken in estimating accurate spatial and temporal discharge throughout the study area.

*Acknowledgements.* The authors thank S. Bartsch for the invaluable technical assistance and hydrologic data collection, monitoring and analysis. We also thank Y. Kim for nutrient, fertilization, gas exchange analysis, and DNDC modeling simulations. We appreciate the interview data collected by P. Poppenborg, T. Nguyen, and S. Trabert. Support from the International Research Training Group TERRECO (GRK 1565/1) funded through the Deutsche Forschungsgemeinschaft (DFG) at the University of Bayreuth is greatly acknowledged.

## References

Abbaspour, K. C.: SWAT-CUP4: SWAT Calibration and Uncertainty Programs – A User Manual, EAWAG Swiss Federal Institute of Aquatic Science and Technology, 103 pp., 2011.

Abbaspour, K. C., Johnson, C. A., and van Genuchten, M. T.: Estimating uncertain flow and transport parameters using a sequential uncertainty fitting procedure, Vadose Zone J., 3, 1340–1352, 2004.

Abbaspour, K. C., Yang, J., Maximov, I., Siber, R., Bogner, K., Mieleitner, J., Zobrist, J., and Srinivasan, R.: Modelling hydrology and water quality in the pre-ailpine/alpine Thur watershed using SWAT, J. Hydrol., 333, 413–430, doi:10.1016/j.jhydrol.2006.09.014, 2007.

Abbaspour, K. C., Faramarzi, M., Ghasemi, S. S., and Yang, H.: Assessing the impact of climate change on water resources in Iran, Water Resour. Res., 45, W10434, doi:10.1029/2008wr007615, 2009.

Allen, R. G., Pereira, L. S., Raes, D., and Smith, M.: Crop Evapotranspiration – Guidlines for Computing Crop Water Requirements, FAO – Food and Agriculture Organization of the United Nations, Rome, ItalyFAO Irrigation and Drainage Paper 56, 300 pp., 1988.





HESSD

10, 7235–7290, 2013



Andersson, J. C. M., Zehnder, A. J. B., Jewitt, G. P. W., and Yang, H.: Water availability, demand and reliability of in situ water harvesting in smallholder rain-fed agriculture in the Thukela River Basin, South Africa, Hydrol. Earth Syst. Sci., 13, 2329–2347, doi:10.5194/hess-13-2329-2009, 2009.

Arnhold, S., Ruidisch, M., Bartsch, S., Shope, C. L., and Huwe, B.: Simulation of runoff patterns and soil erosion on mountainous farmland with and without plastic-covered ridge-furrow cultivation in South Korea, T. ASABE, 56, 667–679, 2013.

Arnold, J. G., Srinivasan, R., Muttiah, R. S., and Williams, J. R.: Large area hydrologic modeling and assessment – Part 1: Model development, J. Am. Water Resour. As., 34, 73–89, doi:10.1111/j.1752-1688.1998.tb05961.x, 1998.

Bartsch, S., Frei, S., Shope, C. L., Peiffer, S., and Fleckenstein, J. H.: River-aquifer exchange fluxes under monsoonal climate conditions, Hydrol. Process., submitted, 2013.

Berka, C., Schreier, H., and Hall, K.: Linking water quality with agricultural intensification in a rural watershed, Water Air Soil Poll., 127, 389–401, doi:10.1023/a:1005233005364, 2001.

Borah, D. K. and Bera, M.: Watershed-scale hydrologic and nonpoint-source pollution models: review of applications, T. ASAE, 47, 789–803, 2004.

Butts, M. B., Payne, J. T., Kristensen, M., and Madsen, H.: An evaluation of the impact of model structure on hydrological modelling uncertainty for streamflow simulation, J. Hydrol., 298, 242–266, 2004.

Calder, I. R.: Hydrologic effects of land use change, in: Handbook of Hydrology, Maidment, D. R., 1992.

Cho, J., Bosch, D., Vellidis, G., Lowrance, R., and Strickland, T.: Multi-site evaluation of hydrology component of swat in the coastal plain of Southwest Georgia, Hydrol. Process., online first, doi:10.1002/hyp.9341, 2012.

Choi, G., Lee, B., Kang, S., and Tenhunen, J.: Variations of Summertime Temperature Lapse Rate within a Mountainous Basin in the Republic of Korea – A case study of Punch Bowl, Yanggu in 2009, available at: http://www.bayceer.uni-bayreuth.de/terreco/en/pub/pub/pub_detail.php?id_obj=90343 (last access: 4 June 2013), 2010.

Dessu, S. B. and Melesse, A. M.: Modelling the rainfall–runoff process of the Mara River basin using the Soil and Water Assessment Tool, Hydrol. Process., 26, 4038–4049, doi:10.1002/hyp.9205, 2012.

Doherty, J.: Ground water model calibration using pilot points and regularization, Ground Water, 41, 170–177, doi:10.1111/j.1745-6584.2003.tb02580.x, 2003.





HESSD
10, 7235–7290, 2013



Duan, Q., Sorooshian, S., Gupta, V., Rousseau, A. N., and Turcotte, R.: Calibration of watershed models, American Geophysical Union, Washington DC, 2003.
Faramarzi, M., Abbaspour, K. C., Schulin, R., and Yang, H.: Modelling blue and green water resources availability in Iran, Hydrol. Process., 23, 486–501, doi:10.1002/hyp.7160, 2009.
Forman, R. T. T. and Alexander, L. E.: Roads and their major ecological effects, Annu. Rev. Ecol. Syst., 29, 207–231, doi:10.1146/annurev.ecolsys.29.1.207, 1998.
Forti, M. C., Neal, C., and Jenkins, A.: Modeling perspective of the deforestation impact in stream water-quality of small preserved forested areas in the amazonian rain-forest, Water Air Soil Poll., 79, 325–337, doi:10.1007/bf01100445, 1995.
Gassman, P. W., Reyes, M. R., Green, C. H., and Arnold, J. G.: The soil and water assessment tool: Historical development, applications, and future research directions, T. ASABE, 50, 1211–1250, 2007.
Goldstein, J. H., Caldarone, G., Duarte, T. K., Ennaanay, D., Hannahs, N., Mendoza, G., Polasky, S., Wolny, S., and Daily, G. C.: Integrating ecosystem-service tradeoffs into land-use decisions, P. Natl. Acad. Sci. USA, 109, 7565–7570, doi:10.1073/pnas.1201040109, 2012.
Green, H. and Ampt, G. A.: Studies on Soil Physics: Part II – The Permeability of an Ideal Soil to Air and Water, J. Agr. Sci., 5, 1–26, doi:10.1017/S0021859600001751, 1912.
Güngör, Ö. and Göncü, S.: Application of the soil and water assessment tool model on the Lower Porsuk Stream Watershed, Hydrol. Process., 27, 453–466, doi:10.1002/hyp.9228, 2013.
Gupta, H. V., Sorooshian, S., and Yapo, P. O.: Status of Automatic Calibration for Hydrologic Models: Comparison with Multilevel Expert Calibration, J. Hydrol. Eng., 4, 135–143, doi:10.1061/(asce)1084-0699(1999)4:2(135), 1999.
Hargreaves, G. H. and Samani, Z. A.: Reference crop evapotranspiration from temperature, Appl. Eng. Agr., 1, 96–99, 1985.
Hellebrand, H. and van den Bos, R.: Investigating processes in the use of spatial discretization of hydrological conceptual rainfall runoff modelling: a case study for the meso-scale, Hydrol. Process., 22, 2943–2952, doi:10.1002/hyp.6909, 2008.
Jha, M., Gassman, P. W., Secchi, S., Gu, R., and Arnold, J.: Effect of watershed subdivision on swat flow, sediment, and nutrient predictions, J. Am. Water Resour. As., 40, 811–825, doi:10.1111/j.1752-1688.2004.tb04460.x, 2004.





HESSD
10, 7235–7290, 2013



Jo, K.-W. and Park, J.-H.: Rapid Release and Changing Sources of Pb in a Mountainous Watershed during Extreme Rainfall Events, Environ. Sci. Technol., 44, 9324–9329, doi:10.1021/es102109a, 2010.

Jun, M.: Device for Reducing Muddy Water in the Watershed of Soyang Dam, Regional Institute of Gangwon, South Korea, 2009.

Jung, B.-J., Lee, H.-J., Jeong, J.-J., Owen, J., Kim, B., Meusburger, K., Alewell, C., Gebauer, G., Shope, C., and Park, J.-H.: Storm pulses and varying sources of hydrologic carbon export from a mountainous watershed, J. Hydrol., 440–441, 90–101, doi:10.1016/j.jhydrol.2012.03.030, 2012.

Khakbaz, B., Imam, B., Hsu, K., and Sorooshian, S.: From lumped to distributed via semi-distributed: Calibration strategies for semi-distributed hydrologic models, J. Hydrol., 418–419, 61–77, doi:10.1016/j.jhydrol.2009.02.021, 2012.

Kim, I., Jeong, G. Y., Park, S., and Tenhunen, J.: Predicted Land Use Change in the Soyang River Basin, South Korea, 2011 TERRECO Science Conference, Karlsruhe Institute of Technology, Garmisch-Partenkirchen, Germany, 2–7 October 2011, 2011.

Krysanova, V., Hattermann, F., and Wechsung, F.: Development of the ecohydrological model SWIM for regional impact studies and vulnerability assessment, Hydrol. Process., 19, 763–783, doi:10.1002/hyp.5619, 2005.

Kumar, M. and Duffy, C. J.: Detecting hydroclimatic change using spatio-temporal analysis of time series in Colorado River Basin, J. Hydrol., 374, 1–15, doi:10.1016/j.jhydrol.2009.03.039, 2009.

Kunstmann, H., Krause, J., and Mayr, S.: Inverse distributed hydrological modelling of Alpine catchments, Hydrol. Earth Syst. Sci., 10, 395–412, doi:10.5194/hess-10-395-2006, 2006.

Kwon, Y. S., Lee, H. H., Han, U., Kim, W. H., Kim, D. J., Kim, D. I., and Youm, S. J.: Terrain analysis of Haean Basin in terms of earth science, Journal of Korean Earth Science Society, 11, 236–241, 1990.

Lam, Q. D., Schmalz, B., and Fohrer, N.: Assessing the spatial and temporal variations of water quality in lowland areas, Northern Germany, J. Hydrol., 438–439, 137–147, doi:10.1016/j.jhydrol.2012.03.011, 2012.

Lee, H. J., Park, J. H., Chun, K. W., and Shope, C. L.: Assessing Climate-Induced Risks to Stream Water Quality in Mountainous Forested Watersheds Using Monitoring Data on Different Timescales, Forest Ecol. Manag., submitted, 2013.





HESSD
10, 7235–7290, 2013



Lee, J. M., Ryu, J. C., Kang, H. W., Kang, H. S., Kum, D. H., Jang, C. H., Choi, J. D., and Lim, K. J.: Evaluation of SWAT Flow and Sediment Estimation and Effects of Soil Erosion Best Management Practices, Journal of the Korean Society of Agricultural Engineers, 54, 99–108, doi:10.5389/KSAE.2012.54.1.099, 2012.

Lee, J. W., Eum, J. S., Kim, B., Jang, W. S., Ryu, J. C., Kang, H. W., Kim, K. S., and Lim, K. J.: Water Quality Prediction at Mandae Watershed using SWAT and Water Quality Improvement with Vegetated Filter Strip, Journal of the Korean Society of Agricultural Engineers, 53, 37–45, doi:10.5389/KSAE.2011.53.1.037, 2011.

Mekonnen, M. A., Worman, A., Dargahi, B., and Gebeyehu, A.: Hydrological modelling of Ethiopian catchments using limited data, Hydrol. Process., 23, 3401–3408, doi:10.1002/hyp.7470, 2009.

Monteith, J. L.: Evaporation and the Environment, in: The state and movement of water in living organisms, edited by: Fogg, G. E., Cambridge University Press, 205–234, 1965.

Moriasi, D. N., Arnold, J. G., Liew, M. W. V., Bingner, R. L., Harmel, R. D., and Veith, T. L.: Model Evaluation Guidelines for Systematic Quantification of Accuracy in Watershed Simulations, T. ASABE, 50, 885–900, 2007.

Murdoch, P. S., Baron, J. S., and Miller, T. L.: Potential effects of climate chance on surface-water quality in North America, J. Am. Water Resour. As., 36, 347–366, doi:10.1111/j.1752-1688.2000.tb04273.x, 2000.

Nash, J. E. and Sutcliffe, J. V.: River Flow Forecasting through Conceptual Models Part 1 – A Discussion of Principles, J. Hydrol. (Amsterdam), 10, 282–290, 1970.

Neitsch, S. L., Arnold, J. G., Kiniry, J. R., Srinivasan, R., and Williams, J. R.: Soil and Water Assessment Tool Input/Output File Documentation Version 2009, Grassland, Soil and Water Research Laboratory, Agricultural Research Service and Blackland Research Center, Texas Agricultural Experiment Station, College Station, Texas, 2010.

Neitsch, S. L., Arnold, J. G., Kiniry, J. R., and Williams, J. R.: Soil and Water Assessment Tool Theoretical Documentation Version 2009, Grassland, Soil and Water Research Laboratory, Agricultural ResearchService and Blackland Research Center, Texas Agricultural Experiment Station, College Station, Texas, 2011.

Nguyen, T., Hoang, V. N., and Seo, B.: Cost and environmental efficiency of rice farms in South Korea, Agr. Econ., 43, 367–376, 2012.





HESSD
10, 7235–7290, 2013



Notter, B., MacMillan, L., Viviroli, D., Weingartner, R., and Liniger, H.-P.: Impacts of environmental change on water resources in the Mt. Kenya region, J. Hydrol., 343, 266–278, doi:10.1016/j.jhydrol.2007.06.022, 2007.

Notter, B., Hurni, H., Wiesmann, U., and Abbaspour, K. C.: Modelling water provision as an ecosystem service in a large East African river basin, Hydrol. Earth Syst. Sci., 16, 69–86, doi:10.5194/hess-16-69-2012, 2012.

Penman, H. L.: Natural Evaporation from Open Water, Bare Soil and Grass, P. Roy. Soc. Lond. A, 193, 120–145, 1948.

Pieri, L., Bittelli, M., Wu, J. Q., Dun, S., Flanagan, D. C., Pisa, P. R., Ventura, F., and Salvatorelli, F.: Using the Water Erosion Prediction Project (WEPP) model to simulate field-observed runoff and erosion in the Apennines mountain range, Italy, J. Hydrol., 336, 84–97, doi:10.1016/j.jhydrol.2006.12.014, 2007.

Priestley, C. H. B. and Taylor, R. J.: On the Assessment of Surface Heat Flux and Evaporation Using Large-Scale Parameters, Mon. Weather Rev., 100, 81–92, 1972.

Rantz, S. E.: Measurement and Computation of Streamflow, in: Vol. 2 – Computation of Discharge, USGS Water Supply Paper 2175, US Geological Survey, Washington, DC, 1982.

Reid, W. V., Chen, D., Goldfarb, L., Hackmann, H., Lee, Y. T., Mokhele, K., Ostrom, E., Raivio, K., Rockstrom, J., Schellnhuber, H. J., and Whyte, A.: Earth System Science for Global Sustainability: Grand Challenges, Science, 330, 916–917, doi:10.1126/science.1196263, 2010.

Ruidisch, M., Kettering, J., Arnhold, S., and Huwe, B.: Modeling water flow in a plastic mulched ridge cultivation system on hillslopes affected by South Korean summer monsoon, Agr. Water Manage., 116, 204-217, doi:10.1016/j.agwat.2012.07.011, 2013.

Schuol, J. and Abbaspour, K. C.: Calibration and uncertainty issues of a hydrological model (SWAT) applied to West Africa, Adv. Geosci., 9, 137–143, doi:10.5194/adgeo-9-137-2006, 2006.

Schuol, J., Abbaspour, K. C., Srinivasan, R., and Yang, H.: Estimation of freshwater availability in the West African sub-continent using the SWAT hydrologic model, J. Hydrol., 352, 30–49, doi:10.1016/j.jhydrol.2007.12.025, 2008a.





HESSD
10, 7235–7290, 2013



Schuol, J., Abbaspour, K. C., Yang, H., Srinivasan, R., and Zehnder, A. J. B.: Modeling blue and green water availability in Africa, Water Resour. Res., 44, W07406, doi:10.1029/2007wr006609, 2008b.
Shope, C. L., Bartsch, S., Kim, K., Kim, B., Tenhunen, J., Peiffer, S., Park, J. H., Ok, Y. S., and Fleckenstein, J., Koellner, T.: A weighted, multi-method approach for accurate basin-wide streamflow estimation in an ungauged watershed, J. Hydrol., 494, 72–82, doi:10.1016/j.jhydrol.2013.04.035, 2013.
Spruill, C. A., Workman, S. R., and Taraba, J. L.: Simulation of daily and monthly stream discharge from small watersheds using the SWAT model, T. ASAE, 43, 1431–1439, 2000.
Stehr, A., Debels, P., Romero, F., and Alcayaga, H.: Hydrological modelling with SWAT under conditions of limited data availability: evaluation of results from a Chilean case study, Hydrolog. Sci. J., 53, 588–601, doi:10.1623/hysj.53.3.588, 2008.
Tenhunen, J., Seo, B., and Lee, B.: Spatial setting of the TERRECO project in the Haean catchment of Yanggu-gun and the Soyang watershed in Gangwan-do, AsiaFlux Training Course on Flux Monitoring: From Theory to Application, Seoul, South Korea, 2011,
Tilman, D., Cassman, K. G., Matson, P. A., Naylor, R., and Polasky, S.: Agricultural sustainability and intensive production practices, Nature, 418, 671–677, doi:10.1038/nature01014, 2002.
Tripathi, M. P., Raghuwanshi, N. S., and Rao, G. P.: Effect of watershed subdivision on simulation of water balance components, Hydrol. Process., 20, 1137–1156, doi:10.1002/hyp.5927, 2006.
U.S.D.A.: Soil Conservation Survey SCS, National Engineering Hand Book, Section 4, in: Hydrology, U.S.D.A, Washington, DC, 1972.
Wilson, C. B., Valdes, J. B., and Rodriguez-Iturbe, I.: On the influence of the spatial distribution of rainfall on storm runoff, Water Resour. Res., 15, 321–328, 1979
Winchell, M., Srinivasan, R., Di Luzio, M., and Arnold, J.: ArcSWAT Version 2009.93.5, Stone Environmental, Inc., Texas A&M Spatial Sciences Laboratory, Blackland Research and Extension Center Austin, Texas, 2010.
Xu, N., Saiers, J. E., Wilson, H. F., and Raymond, P. A.: Simulating streamflow and dissolved organic matter export from a forested watershed, Water Resour. Res., 48, W05519, doi:10.1029/2011wr011423, 2012a.
Xu, Y. D., Fu, B. J., He, C. S., and Gao, G. Y.: Watershed discretization based on multiple factors and its application in the Chinese Loess Plateau, Hydrol. Earth Syst. Sci., 16, 59–68, doi:10.5194/hess-16-59-2012, 2012b.





HESSD
10, 7235–7290, 2013



Yang, J., Reichert, P., Abbaspour, K. C., Xia, J., and Yang, H.: Comparing uncertainty analysis techniques for a SWAT application to the Chaohe Basin in China, J. Hydrol., 358, 1–23, doi:10.1016/j.jhydrol.2008.05.012, 2008.

Yanggu County Office: Yanggu statistical year-book, 2002–2011, Yanggu, Gangwon, Republic of Korea, 2012.





HESSD

10, 7235–7290, 2013



**Table 1.** Principle input datasets for the construction of the Haean catchment SWAT model.

| Dataset | Agency | Dataset Type | Scale |
|---|---|---|---|
| (a) Spatial Datasets | | | |
| General boundaries | GADM[a] | Bathymetry, coastline, roads, lakes, rivers, counties, watersheds | 1 : 10 000 |
| Watershed DEM | NGII[b] | Clipped DEM from Soyang Lake contour map | 1 : 25 000 |
| Stream channels | TERRECO[c] | Hydrologically corrected high-density flow network | 1 : 10 000 |
| Soils | RDA[d] | Clipped from Soyang Lake surficial soils map | 1 : 25 000 |
| Soils | TERRECO[e] | From 2009-2011 field based shallow soil (1.2) m observations | 1 : 10 000 |
| Land cover | TERRECO[f] | Agriculture and Forest field validated LULC | 1 : 5000 |
| (b) Temporal Datasets | | | |
| Precipitation, temperature | KMA[g] | Haean Cooperative Network weather station (1998–2009) | Point |
| Relative humidity, wind speed | KMA[g] | Yanguu Cooperative Network weather station (1998–2009) | Point |
| Solar radiation | KMA[g] | Chuncheon Cooperative Network weather station (1998–2009) | Point |
| Local meteorology | TERRECO[h] | TERRECO stations, 15 in catchment (2009–2011) | Point |
| WWTP point sources | YCO[i] | Wastewater treatment statistics at 5 plants (2002–2010) | Point |
| Discharge and Loads | TERRECO[j] | Field-based, discharge measurements (2003–2011) | Point |
| Agricultural management data | TERRECO[k] | Farmer, county, administrative interviews and field-based plots | |

[a] GADM – Global Administrative Areas. [b] NGII – National Geographic Information Institute. [c] TERRECO – Field-based TERRECO IRTG observations, GPS surveyed perennial and ephemeral stream channels. [d] RDA – Rural Development Administration. [e] TERRECO – Field-based TERRECO IRTG observations, 2009–2011 test pits, soil samples, soil characterization. [f] TERRECO – Field-based TERRECO IRTG observations, 2009 (36 classes), 2010 (114 classes), 2011 (100 classes). [g] KMA – Korean Meteorological Weather Station Network. [h] TERRECO – Field-based TERRECO IRTG observations, 2009–2011 (precipitation, temperature, relative humidity, wind speed, solar radiation. [i] YCO – Yanguu County Office, wastewater treatment statistics 2003–2010. [j] TERRECO – Field-based, spatially distributed, discharge measurements as described in Shope et al. (2013). [k] TERRECO – Field-based, spatially distributed plots of example management and interviews with multiple stakeholders.





HESSD
10, 7235–7290, 2013



**Table 2.** Percentage of Haean catchment associated with the individual aggregated land use, soil, and slope classifications. The slope classification generally defines the difference between forest, dryland farming, and rice paddy systems throughout Haean.

| Category | Area ($km^2$) | Percent Watershed |
|---|---|---|
| *Landuse* | | |
| Barren soil | 5.92 | 9.43 % |
| General beans | 1.63 | 2.60 % |
| Rice | 8.53 | 13.59 % |
| General cabbage | 3.21 | 5.12 % |
| Coniferous forest | 0.04 | 0.06 % |
| Deciduous forest | 35.29 | 56.25 % |
| Ginseng | 0.81 | 1.29 % |
| Inland water | 0.03 | 0.04 % |
| Residential land use | 1.05 | 1.67 % |
| Maize | 0.52 | 0.83 % |
| General orchards | 0.86 | 1.36 % |
| Potato | 2.47 | 3.93 % |
| Radish | 2.12 | 3.38 % |
| Codonopsis | 0.28 | 0.44 % |
| *Soils* | | |
| Flat dry soil | 8.07 | 12.87 % |
| Forest soil | 19.74 | 31.46 % |
| Moderately steep dry soil | 8.33 | 13.28 % |
| Rice paddy soil | 13.78 | 21.96 % |
| Sealed ground | 12.47 | 19.87 % |
| Very steep forest soil | 0.35 | 0.55 % |
| *Slope* | | |
| Low slope rice paddy | 8.02 | 12.79 % |
| Moderate slope dryland | 17.43 | 27.78 % |
| Steep slope forest uplands | 37.28 | 59.43 % |





HESSD
10, 7235–7290, 2013



**Table 3.** Agricultural crop management schedule including planting and harvest dates, fertilization dates, amounts, and type of fertilizer, tilling dates and method, SCS curve number for each crop, and the heat units required to reach maturity.

| LULC/ Crop | CN[a] | PHU[b] (°C) | Tillage JD | Tillage Type | Fertilizer JD | Fertilizer Type[c] | Fertilizer Amnt[d] | Planting (Leaf Out)[e] JD | Harvest (Cessation)[e] JD | Intial Planting Age (yr) | Intial Planting LAI (–) | Intial Planting Biomass (kg ha$^{-1}$) |
|---|---|---|---|---|---|---|---|---|---|---|---|---|
| General | 70.3 | 1710 | 121 | Rotary Hoe | 133 | Chem | 345 | 135 | 224 | | | |
| Bean | | | 133 | Furrow Out | 133 | Org | 120 | | | | | |
| General | 71 | 2159 | 126 | Rotary Hoe | 138 | Chem | 360 | 140 | 201 | | | |
| Cabbage | | | 138 | Furrow Out | 138 | Org | 150 | | | | | |
| | | | | | 171 | Chem | 0.72 | | | | | |
| Potato | 71.8 | 2381 | 101 | Rotary Hoe | 113 | Chem | 330 | 115 | 243 | | | |
| | | | 113 | Furrow Out | 113 | Org | 100 | | | | | |
| Radish | 71.3 | 1631 | 136 | Rotary Hoe | 150 | Chem | 340 | 152 | 232 | | | |
| | | | 150 | Furrow Out | 150 | Org | 150 | | | | | |
| | | | | | 182 | Chem | 150 | | | | | |
| Rice | 78 | 2736 | 124 | Rotary Hoe | 136 | Chem | 230 | 138 | 288 | 0 | 0.2 | 50 |
| | | | 136 | Rice Roller | 156 | Chem | 0.2 | | | | | |
| | | | | | 169 | Chem | 0.2 | | | | | |
| | | | | | 181 | Chem | 0.5 | | | | | |
| | | | | | 193 | Chem | 0.5 | | | | | |
| Ginseng | 71.5 | 3065 | 109 | Rotary Hoe | 121 | Chem | 468 | 123 | 298 | | | |
| | | | 121 | Furrow Out | 121 | Org | 120 | | | | | |
| Maize | 69.7 | 2999 | 111 | Rotary Hoe | 123 | Chem | 316 | 125 | 295 | | | |
| | | | 123 | Furrow Out | 123 | Org | 100 | | | | | |
| General | 58.6 | 3163 | 106 | Rotary Hoe | 118 | Chem | 287 | 120 | 303 | 10 | 0 | 100 |
| Orchard | | | 118 | Furrow Out | 118 | Org | 100 | | | | | |
| Timothy | 72 | 2912 | | | | | | 135 | 304 | | | |
| Codonopsis | 40.7 | 2833 | | | 120 | Chem | 320 | 120 | 307 | | | |
| | | | | | 120 | Org | 150 | | | | | |
| | | | | | 166 | Chem | 0.5 | | | 40 | 0 | 342 |
| Forest | 50.5 | 2896 | | | | | | 112 | 307 | | | |

[a] CN is the SCS curve number. [b] PHU is the cummulative heat units above 0.0 °C required for the LULC/crop to reach maturity. [c] Fertilizer type is classified as Chem (inorganic chemical) not explicitly described or Org (organic manure). [d] Fertilizer amount (kg ha$^{-1}$). [e] Leaf out and cessation define the beginning and end of season for forest and orchard land use.





HESSD
10, 7235–7290, 2013



**Table 4.** Example SWAT model crop parameter database variations in the Haean model.

| LULC | Heat[a] Units | HUSC[b] | BLAI[c] | DLAI[d] | FRGRW1[e] | LAIMX1[f] | FRGRW2[e] | LAIMX2[f] | GSI[g] | T_BASE[h] | ALAI_MIN[i] | HVSTI[j] | CHTMX[k] | BIO_E[l] | BIO_LEAF[m] | BMDIEOFF[n] |
|---|---|---|---|---|---|---|---|---|---|---|---|---|---|---|---|---|
| Rice | 1250 | 0.15 | 4 | 0.95 | 0.1 | 0.1 | 0.5 | 0.95 | 0.005 | 10 | 0 | 0.5 | 0.6 | 22 | 0 | 0.1 |
| Radish | 3300 | 0.01 | 5 | 0.9 | 0.1 | 0.1 | 0.3 | 0.95 | 0.3 | 0 | 0 | 2 | 0.6 | 30 | 0 | 0.1 |
| Potato | 3000 | 0.01 | 4 | 0.9 | 0.1 | 0.1 | 0.5 | 0.95 | 0.003 | 0 | 0 | 0.95 | 0.6 | 25 | 0 | 0.1 |
| General beans | 1050 | 0.15 | 5.4 | 1 | 0.1 | 0.1 | 0.5 | 0.95 | 0.003 | 10 | 0 | 0.31 | 0.6 | 25 | 0 | 0.1 |
| General cabbage | 900 | 0.2 | 3.5 | 0.9 | 0.1 | 0.1 | 0.5 | 0.95 | 0.003 | 0 | 0 | 0.8 | 0.5 | 19 | 0 | 0.1 |
| Deciduous forest | 300 | 0.01 | 7 | 1 | 0.1 | 0.1 | 0.5 | 0.95 | 0.0005 | 0 | 0 | 0.76 | 10 | 15 | 0.15 | 0.1 |
| Coniferous forest | 800 | 0.01 | 7 | 0.97 | 0.1 | 0.1 | 0.5 | 0.95 | 0.0005 | 0 | 0.06 | 0.76 | 10 | 15 | 0.15 | 0.1 |

[a] Heat Units is the total base zero annual heat units for the plant cover/land use to reach maturity. [b] HUSC is the fraction of the total base zero annual heat units at which the management operation occurs. [c] BLAI is the maximum potential leaf area index. [d] DLAI is the fraction of the growing season when the leaf area begins to decline. [e] FRGRW1,2 represent the fraction of the plant growing season corresponding to the 1st and 2nd point on the optimal leaf area development curve. [f] LAIMX 1,2 represent the fraction of the maximum leaf area index corresponding to the 1st and 2nd point on the optimal leaf area development curve. [g] GSI is the maxixmum stomatal conductance at high solar radiation and low vapor pressure deficit ($m\,s^{-1}$). [h] T_BASE is the minimum or base temperature for plant growth (°C). [i] ALAI_MIN is the minimum leaf area index for the plant during the dormant period ($m^2\,m^{-2}$). [j] HVSTI is the fraction of aboveground biomass removed during a harvest operation and lost from the system. [k] CHTMX is the maximum canopy height (m). [l] BIO_E is the radiation use efficiency or biomass energy ratio ($(kg\,ha^{-1})/(MJ\,m^{-2})$). [m] BIO_LEAF is the fraction of tree biomass accumulated each year that is converted to residue during dormancy. [n] BMDIEOFF is the biomass dieoff fraction.





HESSD
10, 7235–7290, 2013



**Table 5.** SWAT parameter sensitivity and significance between discharge parameters throughout the Haean catchment (Fig. 4). Calibrated SWAT parameters for the Haean catchment, including the individual ranking along the elevation based transect, the minimum and maximum parameter values for all subbasins accounted for by each monitoring location, and the average calibrated parameter value. Because of the distributed nature of the Haean model, individual parameters varied depending on crop type, elevation, aspect and therefore, a specific parameter value is not available.

| Parameter | Parameter ranking | | | | | | *p* value (sensitivity of significance) | | | | | | *t* stat (significance magnitude) | | | | | | Minimum–Maximum Parameter Value [Final Average Parameter Value] | | | | |
|---|---|---|---|---|---|---|---|---|---|---|---|---|---|---|---|---|---|---|---|---|---|---|---|
| (distribution) | S1a | S1 | S4W | S5 | S6 | S7 | S1a | S1 | S4w | S5 | S6 | S7 | S1a | S1 | S4w | S5 | S6 | S7 | S1 | S4W | S5 | S6 | S7 |
| *CH_K2.rte (subbasin)* | 13 | 13 | 12 | 13 | 12 | 10 | 0.00 | 0.00 | 0.00 | 0.00 | 0.06 | 0.03 | 16.23 | 6.01 | 6.21 | −6.18 | −1.89 | −2.21 | 81–139 [94] | 43–139 [83] | −51–70 [9.2] | 24–117 [71] | 51–143 [97] |
| *ALPHA_BNK.rte (subbasin)* | 12 | 12 | 8 | 12 | 13 | 11 | 0.00 | 0.00 | 0.00 | 0.00 | 0.02 | 0.00 | −8.77 | −3.68 | −3.18 | 3.10 | 2.34 | 4.94 | 0.01–0.35 [0.34] | 0.05–0.80 [0.22] | 0.15–0.87 [0.51] | 0.28–0.92 [0.60] | 0.42–1.25 [0.83] |
| *CH_N2.rte (subbasin)* | 11 | 9 | 11 | 11 | 9 | 9 | 0.00 | 0.39 | 0.07 | 0.43 | 0.64 | 0.21 | 4.44 | 0.87 | 1.79 | −0.79 | 0.46 | 1.27 | 0.13–0.39 [0.26] | 0.08–0.31 [0.17] | 0.03–0.22 [0.12] | 0.08–0.30 [0.19] | 0.06–0.29 [0.17] |
| *CN2.mgt (land use, subbasin)* | 10 | 11 | 10 | 9 | 5 | 4 | 0.15 | 0.11 | 0.81 | 0.66 | 0.01 | 0.50 | 1.43 | 1.62 | 0.24 | 0.44 | −2.51 | 0.67 | −0.62–0.23 [-0.58] | −0.55–0.36 [-0.05] | −0.32–0.54 [0.11] | −0.33–0.60 [0.14] | −0.38–0.52 [0.07] |
| *ESCO.hru (land use, subbasin)* | 9 | 7 | 6 | 5 | 3 | 2 | 0.21 | 0.42 | 0.13 | 0.21 | 0.52 | 0.99 | −1.24 | 0.81 | 1.51 | 1.26 | −0.64 | −0.01 | 0.19–0.89 [0.39] | 0.16–0.91 [0.55] | 0.25–1.01 [0.63] | 0.13–0.89 [0.51] | 0.21–0.97 [0.59] |
| *GW_REVAP.gw (soil type, subbasin)* | 8 | 6 | 1 | 1 | 2 | 5 | 0.15 | 0.30 | 1.00 | 0.60 | 0.55 | 0.42 | 1.45 | 1.05 | 0.00 | −0.53 | 0.60 | 0.80 | 0.06–0.16 [0.09] | 0.05–0.18 [0.09] | 0.03–0.15 [0.09] | 0.02–0.16 [0.09] | 0.03–0.16 [0.10] |
| *GWQMN.gw (soil type, subbasin)* | 7 | 2 | 5 | 4 | 4 | 7 | 0.41 | 0.60 | 0.14 | 0.04 | 0.76 | 0.12 | −0.82 | 0.52 | −1.48 | −2.02 | 0.30 | −1.57 | 32–4151 [475] | 1370–4800 [2675] | 512–3596 [2054] | 323–3894 [2108] | 1133–4890 [3011] |
| *ALPHA_BF.gw (soil type, subbasin)* | 6 | 1 | | 6 | 6 | 8 | 0.77 | 0.81 | | 0.20 | 0.71 | 0.93 | −0.29 | 0.24 | | −1.29 | −0.37 | −0.08 | 0.12–0.46 [0.20] | 0.11–0.52 [0.22] | 0.02–0.39 [0.21] | 0.00–0.38 [0.19] | 0.08–0.46 [0.27] |
| *SOL_K(1).sol (subbasin)* | 5 | 3 | 9 | 10 | 1 | 6 | 0.88 | 0.61 | 0.52 | 0.35 | 0.75 | 0.03 | −0.15 | 0.51 | −0.65 | 0.94 | 0.32 | 2.25 | −1.46–0.22 [−0.78] | −0.56–0.71 [0.10] | −0.64–0.85 [0.10] | −0.90–0.42 [−0.24] | −0.85–0.56 [−0.15] |
| *SOL_AWC(1).sol (subbasin)* | 4 | 10 | 4 | 3 | 10 | | 0.22 | 0.43 | 1.00 | 0.73 | 0.13 | | −1.23 | −0.79 | 0.00 | −0.35 | 1.51 | | −0.20–0.39 [0.30] | −0.41–0.47 [0.02] | −0.56–0.21 [−0.17] | −0.49–0.48 [−0.01] | −0.67–0.18 [−0.25] |
| *REVAPMN.gw (soil type, subbasin)* | 3 | 4 | 7 | 7 | 7 | 1 | 0.43 | 0.69 | 0.72 | 0.79 | 0.58 | 0.95 | 0.80 | −0.41 | 0.36 | 0.27 | −0.56 | −0.06 | 2.73–6.74 [4.72] | 1.98–9.53 [6.14] | 0.41–8.62 [4.51] | 1.42–8.36 [4.89] | 1.62–9.13 [5.38] |
| *GW_DELAY.gw (soil type, subbasin)* | 2 | 5 | 3 | 8 | 8 | 3 | 0.59 | 0.39 | 0.23 | 0.36 | 0.51 | 0.67 | −0.53 | 0.88 | −1.19 | −0.91 | 0.66 | 0.42 | 138–453 [398] | 16–334 [202] | 73–412 [242] | −28–322 [147] | 31–362 [197] |
| *SOL_BD(1).sol (subbasin)* | 1 | 8 | 2 | 2 | 11 | | 0.90 | 0.07 | 0.66 | 0.47 | 0.13 | | −0.13 | 1.85 | 0.44 | 0.72 | 1.53 | | −0.36–0.44 [−0.25] | −0.43–0.30 [−0.05] | −0.62–0.13 [−0.25] | −0.34–0.36 [0.01] | −0.34–0.35 [0.01] |





HESSD
10, 7235–7290, 2013



**Table 6.** Calibration and validation statistics for each of the monitoring locations throughout the Haean Catchment. The data includes the subbasin demarcation of the monitoring locations, the total number of observations, the observed and simulated water balance, the NSE, R2, and PBIAS statistics, and the percent baseflow contribution.

| Monitoring Location | Drainage Area ($km^2$) | No. of Observ. | NSE | $R^2$ | PBIAS (%) | Percent Baseflow |
|---|---|---|---|---|---|---|
| *2010 calibration period* | | | | | | |
| S1 | 0.35 | 283 | 0.83 | 0.84 | 9.61 | 0.49 |
| SD | 1.54 | 33 | 0.90 | 0.91 | −8.78 | 0.16 |
| S4 | 1.66 | 202 | 0.95 | 0.96 | 8.86 | 0.42 |
| S5 | 2.09 | 259 | 0.85 | 0.89 | 1.27 | 0.16 |
| SN | 3.12 | 34 | 0.95 | 0.96 | −1.08 | 0.13 |
| SS | 6.55 | 36 | 0.85 | 0.95 | −72.38 | 0.21 |
| SW | 6.65 | 35 | 0.97 | 0.98 | −10.60 | 0.13 |
| SK | 7.28 | 35 | 0.95 | 0.97 | −6.93 | 0.20 |
| S6 | 22.15 | 267 | 0.64 | 0.70 | 41.33 | 0.06 |
| S7 | 52.08 | 207 | 0.73 | 0.93 | 29.39 | 0.13 |
| *2009 validation period* | | | | | | |
| S1 | 0.35 | 66 | 0.92 | 0.83 | −6.85 | 0.54 |
| SD | 1.54 | 20 | 0.98 | 0.97 | −9.05 | 0.15 |
| S4 | 1.66 | 0 | – | – | – | – |
| S5 | 2.09 | 65 | 0.88 | 0.90 | −3.18 | 0.18 |
| SN | 3.12 | 22 | 0.91 | 0.94 | −14.47 | 0.14 |
| SS | 6.55 | 22 | 0.76 | 0.87 | −33.31 | 0.20 |
| SW | 6.65 | 22 | 0.94 | 0.95 | −3.59 | 0.10 |
| SK | 7.28 | 22 | 0.62 | 0.71 | 19.76 | 0.26 |
| S6 | 22.15 | 0 | – | – | – | – |
| S7 | 52.08 | 22 | 0.74 | 0.97 | 26.30 | 0.13 |





HESSD
10, 7235–7290, 2013



**Table 7.** Biomass production and crop yield statistics for South Korea and specifically, for the Haean catchment.

| | Average S Korea Cultivation | | | 2009 Haean | 2009 LULC Area | | 2009 Haean |
|---|---|---|---|---|---|---|---|
| | Area (ha) | Production (metric tn) | Yield (tn ha$^{-1}$) | Plot Yield (tn ha$^{-1}$) | Plot (ha) | Haean (ha) | Crop Yield (tn) |
| Rice | 936 766 | 6 869 305 | 7.33 | 11.26 | 13.32 | 87 312 | 73 796 |
| Cabbage | 34 321 | 2 542 000 | 74.07 | 4.81 | 10.35 | 32 742 | 15 226 |
| Potato | 26 804 | 600 000 | 22.38 | 22.94 | 1.17 | 25,038 | 490 895 |
| Radish | 23 780 | 1 223 000 | 51.43 | 35.24 | 1.26 | 21 828 | 610 422 |
| Soybean | 80 505 | 137 000 | 1.70 | 14.66 | 0.09 | 16 692 | 2 719 127 |
| Deciduous Forest | – | – | – | 42.03 | 103.05 | 359 520 | 146 620 |

Sources: Ministry for Food, Agriculture, Forestry & Fisheries (MIFAFF), Korea Rural Economic Institute, Korean Statistical Information Service (KOSIS), Korea Agro-Fisheries Trade Corp. (aT), Yanggu statististical year-book 2003–2011 from the Yanggu County Office, FAOSTAT 2008, World Bank 2009.





HESSD
10, 7235–7290, 2013



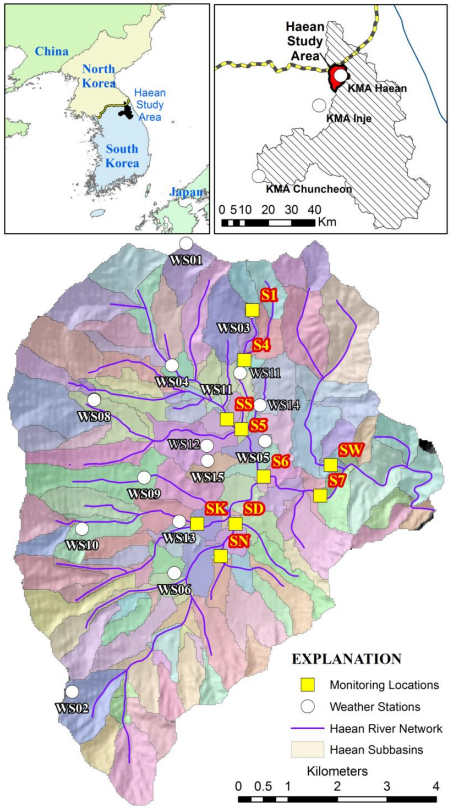


**Fig. 1.** Haean study area within the Lake Soyang watershed is located in northeastern South Korea along the demilitarized zone (DMZ) border with North Korea. The regional KMA weather station and local meteorological stations are denoted with white circles and (WS). River discharge monitoring locations are denoted by (S) and the yellow squares.





HESSD
10, 7235–7290, 2013



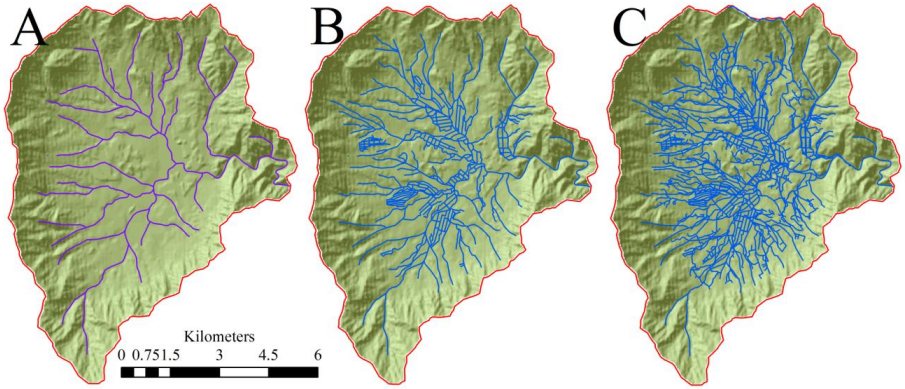


**Fig. 2.** Multiple river system and infrastructure model configurations within the Haean catchment which, contribute to surface discharge accumulation and flow routing. The panels display the configuration for **(A)** solely the Haean river network, **(B)** the river network and engineered culvert drainage system, and **(C)** the river network, the culvert system, and the road infrastructure.





HESSD
10, 7235–7290, 2013



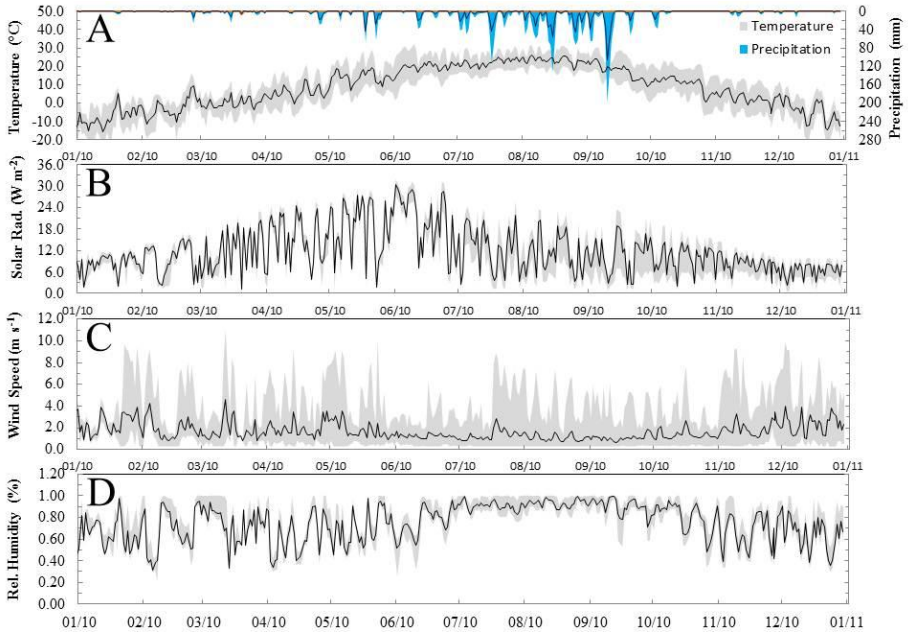


**Fig. 3.** Meteorologic variability and average daily value of each variable throughout the Haean catchment for 2010. **(A)** describes the daily precipitation and temperature variability, **(B)** is the range in solar radiation and the average value between all of the locations, **(C)** is the wind speed variability, and **(D)** is the relative humidity range.





HESSD
10, 7235–7290, 2013



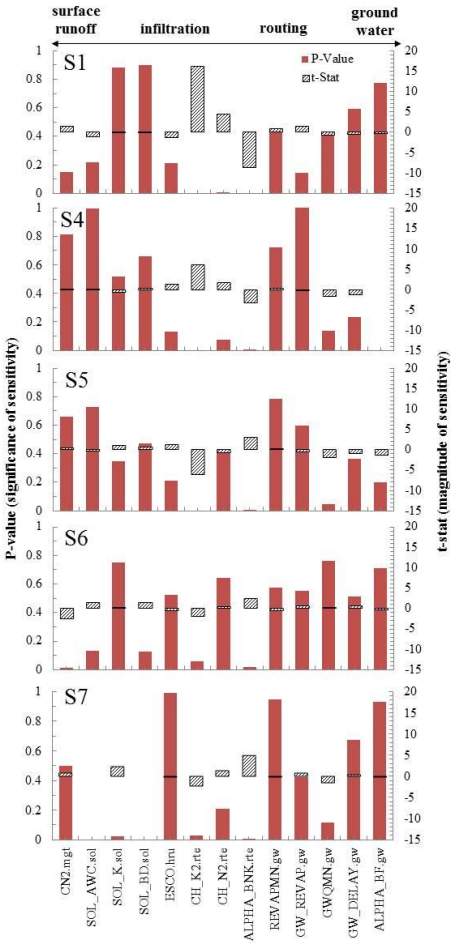


**Fig. 4.** SWAT simulated parameter sensitivity ($p$ value) and model significance ($t$ test) for the Haean catchment for monitoring locations S1, S4, S5, S6, and S7 along the elevation transect.





HESSD
10, 7235–7290, 2013



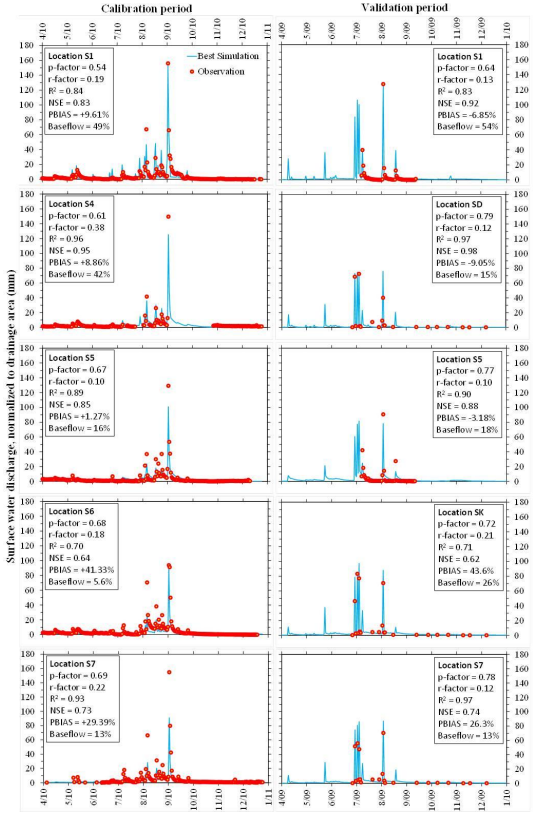


**Fig. 5.** Calibrated and validated daily comparison of drainage area normalized observed and simulated river discharge along the elevation transect of monitoring locations S1, S4, S5, S6, and the catchment outlet S7. Included on each panel are the objective function and optimization statistics.





HESSD
10, 7235–7290, 2013



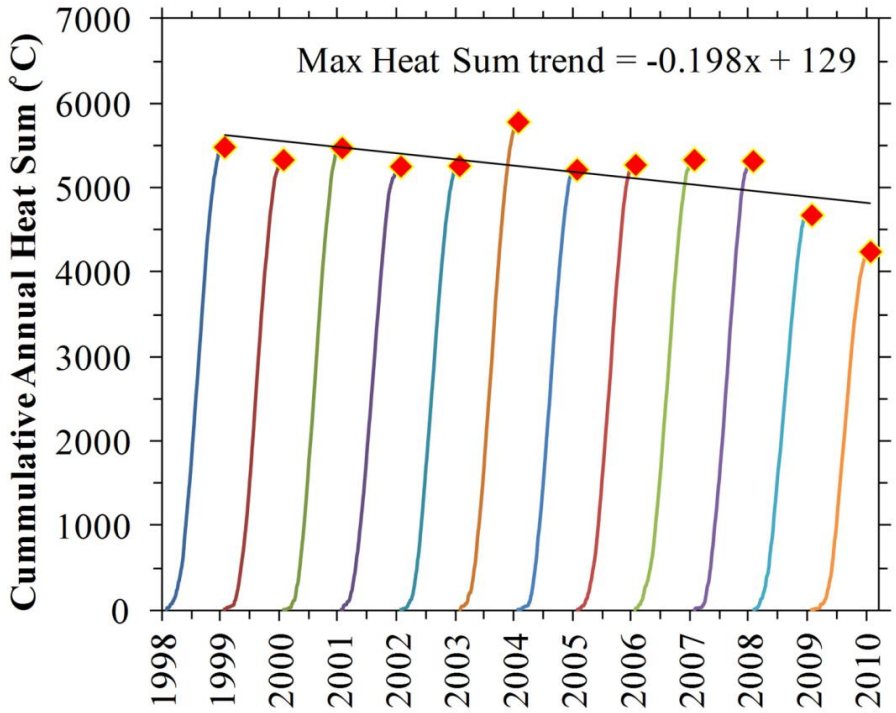


**Fig. 6.** Daily heat sum estimate between 1998 and 2010 for the S1 forest boundary monitoring location within the Haean watershed (Fig. 1).





HESSD
10, 7235–7290, 2013



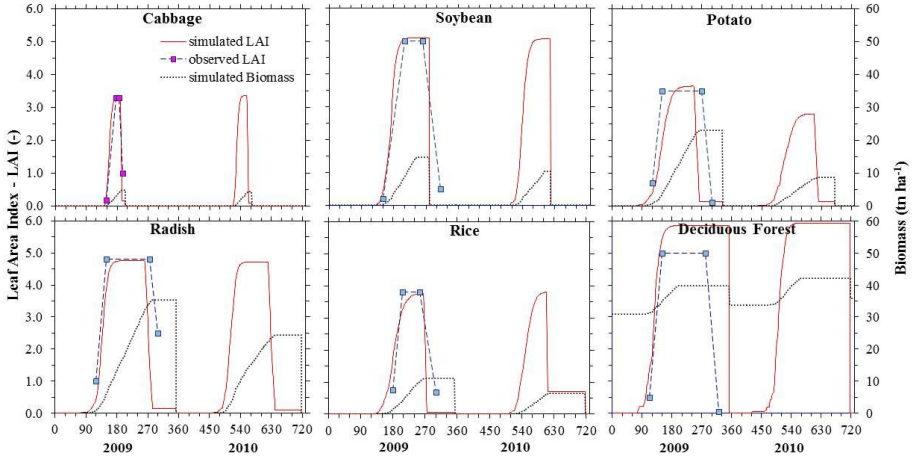


**Fig. 7.** Comparison of simulated versus observed leaf area index (LAI) for five of the primary crops grown in Haean and the deciduous forest.





HESSD
10, 7235–7290, 2013